# A new Perspective on the Evolution of Water Vapor Channel Brightness Temperatures in a Warming Climate

submitted by
Laura Jasmin Dietrich

Master's thesis in Meteorology
MIN-Fakultät
Universität Hamburg

August 1, 2019

1st Supervisor: Prof. Dr. Stefan Bühler
Meteorologisches Institut, Universität Hamburg
2nd Supervisor: Lukas Kluft
Max-Planck-Institut für Meteorologie
Meteorologisches Institut, Universität Hamburg

**Thema der Arbeit**

Understanding the Changes in Brightness Temperature in a Warming Climate

# Abstract

Water vapor in the upper troposphere has a strong impact on the Earth's radiation budget. In a warming climate, upper tropospheric water vapor is responsible for one of the largest positive clear-sky feedbacks and therefore it is essential to improve the understanding of its changes. A measure of water vapor in the upper troposphere is the brightness temperature ($T_B$) for water vapor channels. In a conventional view, $T_B$ corresponds to the relative humidity, averaged over an appropriate layer in the upper troposphere.

I develop a new perspective, explaining changes in $T_B$ by a vertical stretching of the temperature ($T$) and specific humidity ($q$) profiles. I show that stretching the profiles describes a major part of the profiles' evolution in a warming climate in the MPI-ESM-LR. I find a strong correlation between the change in $T_B$ and the difference of the stretching parameters for $T$ and $q$ as a robust feature across the CMIP5 ensemble. Even though the relationship differs, the correlation is robust for two simulated measurement instruments AMSU-B and HIRS. The robustness across the CMIP5 ensemble and across two different measurement instruments open a new perspective which allows to interpret changes in $T_B$ not only as a function of a change in relative humidity but also as a consequence of a different evolution of the $T$ and $q$ profiles.

# Contents

# List of Figures

# Chapter 1

# Introduction

Water vapor is the most important greenhouse gas in the Earth's atmosphere (Raval and Ramanathan, 1989). Therefore, a large part of the Earth's outgoing longwave radiation is influenced by the amount of atmospheric water vapor (Held and Soden, 2000; Huang et al., 2007). In a warming climate, the amount of water vapor is projected to increase (Randall et al., 2007; Trenberth et al., 2005). This leads to a large positive feedback which has the potential to nearly double the initial warming (Soden and Held, 2006; Manabe and Wetherald, 1967). Although the major amount of atmospheric water vapor is found in the lower and middle troposphere, it is the upper tropospheric water vapor which is most important for the outgoing longwave radiation (Spencer and Braswell, 1997; Held and Soden, 2000). It is therefore essential to understand the changes of water vapor in the upper troposphere.

A measure of water vapor in the upper troposphere and its impact on the Earth's energy budget is the brightness temperature ($T_B$) for water vapor channels (Dalu, 1986). It corresponds to the weighted mean temperature ($T$) within an emission layer in the upper troposphere. The exact position of this emission layer depends on the amount of water vapor, which corresponds to the specific humidity ($q$).

There are long and robust time series of satellite measurements of $T_B$. The longest of such time series have been measured with the High-resolution Infrared Radiation Sounder (HIRS, Robel et al. (2009) and Shi and Bates (2011)), starting in 1979, and the Advanced Microwave Sounding Unit-B (AMSU-B, (Saunders et al., 1995)), starting in 1998. In this thesis I develop a conceptual model to explain changes in $T_B$ in a warming climate, simulated for these two measurement instruments.

A change in $T_B$ ($\Delta T_B$) can be influenced by both a change in the $T$ profile and a change in the $q$ profile. An increase in $T$ causes an increase of the mean temperature in the emission layer and therefore an increase in $T_B$. An increase in $q$ causes an upward shift of the emission layer to lower temperatures and therefore a decrease in $T_B$. Furthermore, other factors like the $T$ and $q$ profiles' lapse rate have an influence on $\Delta T_B$.

The traditional view of $T_B$ is that it corresponds to the relative humidity (RH) in the upper troposphere (Soden et al., 2005). Keeping the relative humidity constant, an increase in $T$ entails an increase in $q$. The opposing effects of $T$ and $q$ on $T_B$ are then assumed to approximately compensate each other (Soden and Bretherton, 1993). Consequently, an increase in RH decreases $T_B$ and vice versa. Therefore, $T_B$ is used to calculate the upper tropospheric humidity (UTH), which is defined as the weighted mean of RH within the emission layer of $T_B$ (Soden and Bretherton, 1993). Because on average, RH is projected to remain approximately constant in a warming climate (Soden and Held, 2006; Dessler et al., 2008), $T_B$ is expected to remain largely constant as well.

The difficulty with this way of interpreting $T_B$ is that in a warming climate the tropospheric profiles stretch in such a way that the tropopause moves upward (O'Gorman and Singh, 2013). This also applies to the levels of a given absolute humidity. The traditional view on $T_B$, although not incorrect, obscures this important fundamental mode of change.

I develop a new perspective on $\Delta T_B$ by connecting it directly to changes in the $T$ and $q$ profiles. To do so, I simplify the complex evolution of the profiles by the process of vertical stretching. Vertical stretching is able to explain a major part of the profile's evolution in simulations of climate models (Singh and O'Gorman, 2012). The novelty of this perspective is that it does not connect $\Delta T_B$ to a change in the atmospheric parameters, but rather to a process which causes a large part of the changes in the atmospheric parameters. This process provides a new framework for interpreting $\Delta T_B$.

The following Chapter 2 gives information about the brightness temperature and the stretching method to approximate the profiles' evolution. In Chapter 3 I will investigate the new perspective on $\Delta T_B$ in an idealized experiment. The new perspective is tested for model data in Chapter 4, first for the Max Planck Institute Earth System Model (MPI-ESM, Giorgetta et al. (2013)) in low-resolution configuration (LR). Then, I investigate the robustness of the new perspective across 19 further models which are part of the fifth phase of the Coupled Model Intercomparison Project Phase 5 (CMIP5, Taylor et al. (2012)). Finally, I analyze the influence of the measurement instrument on the new perspective in Chapter 5.

# Chapter 2

# Methods and data

## 2.1 Brightness temperature

The brightness temperature ($T_B$) is derived from satellite measurements of the Earth's emission of radiation in a certain frequency range. $T_B$ corresponds to the weighted mean of the temperature $T$ within an emission layer. I investigate changes in $T_B$ for water vapor channel frequencies. For those frequencies, the radiation is mainly absorbed by water vapor. Therefore, the position of the emission layer depends on the amount of water vapor which corresponds to the specific humidity $q$. As a consequence, $T_B$ can be used to derive humidity information (Soden and Bretherton, 1993).

The emission layer from which the major part of the emitted radiation for $T_B$ originates, is located in the upper troposphere (Thomas and Stamnes, 2002). Below this layer, even though the concentration of water vapor is much higher, the emitted radiation is largely absorbed on its way up to the top of the atmosphere and only a small fraction is detected by the satellite. Above this layer, the concentration of water vapor is very low and thus the amount of emitted radiation is low, too. It is assumed, that most of the measured signal originates from a rather thin layer where the optical thickness of the atmosphere reaches one (Thomas and Stamnes, 2002).

Higher values of $q$ increase the optical thickness and the emission layer shifts up to lower $T$. Thus, an increase in $q$ decreases the measured $T_B$. In a warming climate, the tropical average of the relative humidity of the upper troposphere is assumed to remain approximately constant (Soden and Held, 2006; Dessler et al., 2008). As a consequence, $q$ has to increase. The corresponding upward shift of the emission layer approximately balances out the increase in $T$ so that $T_B$ remains constant, too. Therefore, the traditional view is that $\Delta T_B$ describes a change in the upper tropospheric relative humidity (UTH). I develop a new perspective, explaining changes in $T_B$ by changes in the single $T$ and $q$ profiles.

To simulate $T_B$ for model atmospheres, a radiative transfer model is needed. Radiative transfer models calculate the interaction of electromagnetic radiation with the atmosphere. Given atmospheric profiles as input, they simulate $T_B$ measured by satellite-based instruments from space accounting for the specific instrument properties. I calculate the clear-sky $T_B$ with RTTOV (**R**adiative **T**ransfer for **T**elevision and Infrared Observation Satellite **O**perational **V**ertical Sounder, Saunders et al., 2018), a fast radiative transfer model which simulates $T_B$ with low computational effort by using a band-transmission method. This means that the calculations are not performed for single frequencies, but instead, several frequencies are treated as bands with the same absorption properties. For the results in Chapter 3 and 4, I simulate $T_B$ for the water vapor channel 18 of the microwave instrument AMSU-B (Advanced Microwave Sounding Unit-B, Robel et al., 2009; Saunders et al., 1995). The channel is located at $183.31 \pm 1$ GHz around the peak of a water vapor

absorption line and has a total bandwidth of 1 GHz (Robel et al., 2009). In Chapter 5, I compare my results to the simulated $T_B$ for the infrared instrument HIRS (High-resolution Infrared Radiation Sounder, Robel et al., 2009). The water vapor channel for HIRS is located at 6.7 $\mu$m and has a much broader bandwidth of 87.6 $\mathrm{cm}^{-1}$ ($\approx$ 2600 GHz).

A recent study by Lang (2019) detected differences in the simulated $T_B$ for the 1pctCO2 run of the MPI-ESM-LR calculated with different radiative transfer models of up to 2.5 K. In the study, calculations of $T_B$ with RTTOV were compared to calculations with the radiative transfer model ARTS (The Atmospheric Radiative Transfer Simulator, Buehler et al., 2018; Buehler et al., 2005; Eriksson et al., 2011). The difference between ARTS and RTTOV increases for decreasing $T_B$ (Figure 2.1a). In a subsequent joint investigation we were able to trace this differences back to the ability of both transfer models to handle the relatively coarse vertical resolution for the CMIP5 models. A coarse vertical resolution causes both ARTS and RTTOV to underestimate the simulated $T_B$. This effect appears to be stronger for RTTOV than for ARTS and produces the difference in $T_B$. We were able to reduce this difference by re-interpolating the profiles linearly to a higher vertical resolution of 97 levels (Figure 2.1b).

In my thesis I only use $T_B$ calculated with RTTOV. As the results for RTTOV are not compared to other radiative transfer models in this thesis and due to the high computational costs of calculating the results of all models for a higher vertical grid resolution, I decided to not re-interpolate the data. This should be kept in mind when comparing absolute values of $\Delta T_B$ to calculations with other radiative transfer models.

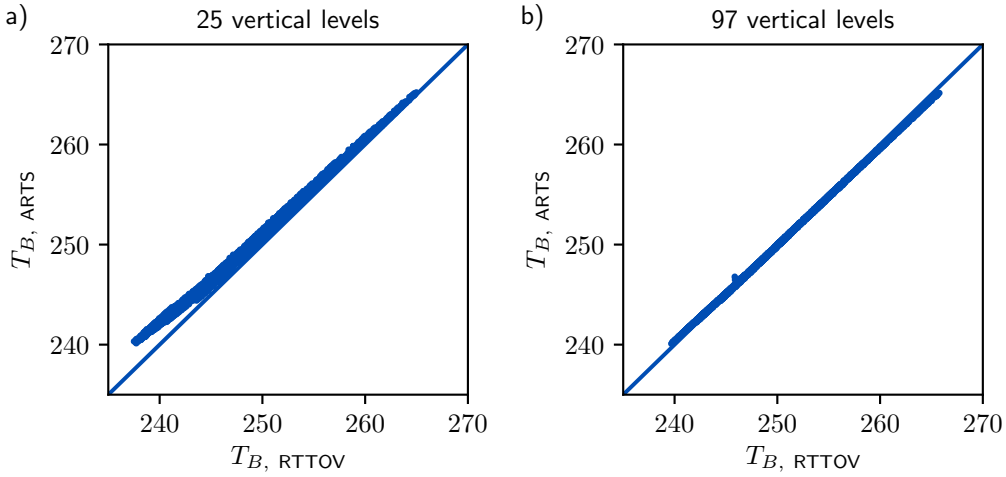


FIGURE 2.1: Brightness temperature for all tropical grid points for the first month of the 1pctCO2 run in the climate model MPI-ESM-LR, calculated with the radiative transfer model ARTS ($T_{B,\mathrm{ARTS}}$) scattered against calculated with the radiative transfer model RTTOV ($T_{B,\mathrm{RTTOV}}$) for the original vertical resolution of 25 levels (left panel) and for data interpolated on 97 vertical levels (right panel).

## 2.2 Stretching method

Previous studies have shown that the evolution of the mean atmospheric profiles in a warming climate is close to an upward shift of the initial profiles (Zelinka and Hartmann, 2010; Kushner et al., 2001; Singh and O'Gorman, 2012; O'Gorman and Singh, 2013). Therefore, I simplify the $T$ and $q$ profiles' evolution in this thesis by vertically stretching them. The method I use for the vertical stretching of the profiles is based on Singh and O'Gorman (2012). Given control profiles of $T$ and $q$, I stretch these profiles by interpolating $T$ and $q$ to new pressure levels. The stretched profiles $T'$ and $q'$ are calculated as

$$T'(p) = T(\beta_T p) \tag{2.1}$$
$$q'(p) = q(\beta_q p). \tag{2.2}$$

The degree of stretching is determined by the stretching parameters $\beta_T$ and $\beta_q$ for $T$ and $q$, respectively. As illustrated in Figure 2.2 for $T$, the value of $T'$ at $p$ corresponds to the value of $T$ at $p + \Delta p$. The difference in pressure $\Delta p$ depends on $\beta_T$:

$$\Delta p = \beta_T p - p = p(\beta_T - 1). \tag{2.3}$$

In their study, Singh and O'Gorman (2012) used one fixed stretching parameter to stretch all $T$ and $q$ profiles. As will be shown in Chapter 4, the profiles of $T$ and $q$ can evolve differently for one grid cell. Therefore, I decided to use individual stretching parameters of $T$ and $q$. Furthermore, I calculate the optimal stretching parameters for each individual grid cell instead of stretching all profiles homogeneously. Note that an equal stretching of both profiles does not correspond to a constant relative humidity.

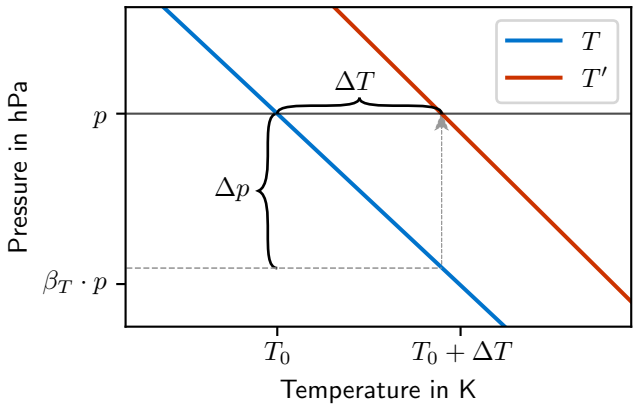


FIGURE 2.2: Illustration of the stretching method for the control temperature profile ($T$, blue line) and the stretched temperature profile ($T'$, red line). $\Delta T$ is the difference between the value of the control temperature profile $T_0$ at the pressure level $p$ and the value of the control temperature profile at the pressure level $p \cdot \beta_T$, depending on the vertical stretching parameter $\beta_T$.

### 2.2.1 Connection to UTH

As already mentioned in Section 2.1, the traditional approach to interpret $T_B$ is to derive information about the UTH. In this section I connect the UTH to a change in $T_B$ caused by stretching the $T$ and $q$ profiles. I do so by drawing a rough connection between $\Delta T_B$

and the difference of the stretching parameters $\beta_q - \beta_T$.

The UTH is defined as the relative humidity RH averaged over the emission layer of $T_B$. It is derived from $T_B$ using a simple relation which was first derived by Soden and Bretherton (1993):

$$\ln(\mathsf{UTH}) = a + bT_B, \tag{2.4}$$

where $a$ and $b$ are constants which are empirically determined. For AMSU-B $a$ and $b$ can be looked up in Buehler and John (2005).

Because UTH is assumed to be RH in the emission layer, and because of the natural logarithm in Equation 2.4, a change in $T_B$ is proportional to the relative change in RH in the emission layer:

$$\Delta T_B \sim \frac{\Delta\mathsf{RH}}{\mathsf{RH}}, \tag{2.5}$$

where $\Delta$ denotes the difference between two profiles at one pressure level. RH is the ratio of the partial pressure of water vapor in the air $e$ and the water vapor pressure of saturation $e_s$:

$$\mathsf{RH} = \frac{e}{e_s}. \tag{2.6}$$

Assuming, that the mass of the humid air $m_h$ can be approximated by the mass of dry air $m_d$, the specific humidity $q$ can be written as

$$q = \frac{m_v}{m_h} \approx \frac{m_v}{m_d} = \frac{\rho_v}{\rho_d}, \tag{2.7}$$

where $m_v$ denotes the mass of water vapor in the air and $\rho_v$ and $\rho_d$ are the partial densities of water vapor and dry air, respectively. Applying the ideal gas law (IGL), $e$ can be written as

$$e = \rho_v R_v T \overset{(2.7)}{=} q\,\rho_d R_v T \overset{(IGL)}{=} q\,p \cdot \frac{R_v}{R_d}, \tag{2.8}$$

where $R_v/R_d \approx 0.622$ is the ratio of the specific gas constants for water vapor and dry air, respectively. Inserting Equation 2.8 into Equation 2.6 gives

$$\mathsf{RH}(p, q, T) = \frac{q\,p}{e_s(T)} \cdot \frac{R_v}{R_d} \tag{2.9}$$

and the relative change of RH from Equation 2.5 at a constant pressure level $p$ turns to

$$\frac{\Delta\mathsf{RH}}{\mathsf{RH}} = \frac{\Delta(\frac{q}{e_s(T)})}{\frac{q}{e_s(T)}} \overset{*}{=} \frac{e_s(T)\Delta q - q\Delta e_s(T)}{q e_s} = \frac{\Delta q}{q} - \frac{\Delta e_s}{e_s}, \tag{2.10}$$

using the Quotient Rule in $*$. Using Clausius Clapeyron's equation

$$\Delta e_s = \frac{Q_v e_s}{R_v T^2}\Delta T, \tag{2.11}$$

where $Q_v$ denotes the heat of condensation, Equation 2.10 can be written as

$$\Delta T_B \sim \frac{\Delta\mathsf{RH}}{\mathsf{RH}} = \frac{\Delta q}{q} - \frac{\Delta T}{T}\frac{Q_v}{T R_v}, \tag{2.12}$$

connecting $\Delta T_B$ to the difference of the relative change in $q$ and the relative change in $T$.

After having found an approximate expression of $\Delta T_B$ which depends on $T$ and $q$, I derive an expression for the stretching parameters which can be used to connect them to $\Delta T_B$. As illustrated in Figure 2.2, the change in $T$ due to a stretching of the profile at one pressure level depends on the lapse rate at this level. Assuming linearity of the $T$ profile between two pressure levels, the temperature lapse rate $\Gamma_T$ is calculated by

$$\Gamma_T = \frac{\Delta_z T}{\Delta_z p}, \tag{2.13}$$

where $\Delta_z$ denotes the vertical difference within one profile. For a vertical stretching the ratio between the pressure shift $\Delta p$ from Equation 2.3 and the change in the $T$ profile $\Delta T$ is equal to $\Gamma_T$:

$$\Gamma_T = \frac{\Delta T}{\Delta p}. \tag{2.14}$$

Thus the change in $T$, resulting from a vertical stretching, gives

$$\Delta T = \Gamma_T \Delta p = \Gamma_T p(\beta_T - 1). \tag{2.15}$$

After rearranging Equation 2.15, the stretching parameter $\beta_T$ at the pressure level $p$ is represented by

$$\beta_T = \frac{\Delta T}{\Gamma_T p} + 1. \tag{2.16}$$

Similarly, the stretching parameter $\beta_q$ can be written as

$$\beta_q = \frac{\Delta q}{\Gamma_q p} + 1, \tag{2.17}$$

where $\Gamma_q$ denotes the lapse rate of $q$.

With regards to the connection of the stretching parameters and $\Delta T_B$, it is the difference between the stretching parameters

$$\beta_q - \beta_T = \frac{\Delta q}{\Gamma_q p} - \frac{\Delta T}{\Gamma_T p}, \tag{2.18}$$

which has a form similar to Equation 2.5. Therefore, I expect $\Delta T_B$ to be dependent on the difference of the stretching parameters.

To open a new perspective on $\Delta T_B$ the aim of this section was to find a relationship between the conceptual model of vertical stretching and the traditional view that $T_B$ is described by the UTH. I found the difference of the stretching parameters $\beta_q - \beta_T$ to best describe $\Delta T_B$ in this context. Using this connection to the traditional view, I expect to find a relationship between the difference in the stretching parameters and $\Delta T_B$.

### 2.2.2 Optimization of the stretching parameters

The new perspective on $T_B$ is that it can be explained by the vertical stretching of the initial $T$ and $q$ profiles (2.1). In order to apply this new perspective to model data, I need

to determine the stretching parameters which best describe the change of the control profiles to the profiles in a warmer climate, called warm profiles hereafter.

As illustrated in Figure 2.3, I determine the optimal stretching parameters by minimizing the RMSE (Root-Mean-Square Error) between the stretched control profile and the warm profile within an optimization layer between $p_0 = 400$ and $p_1 = 200$ hPa:

$$\text{RMSE} = \sqrt{\frac{1}{N} \sum_{p=p_0}^{p_1} \left( x_{\text{stretched}}(p) - x_{\text{warm}}(p) \right)^2}, \tag{2.19}$$

where $x_{\text{stretched}}$ and $x_{\text{warm}}$ are values for $q$ or $T$ of the stretched and the warm profile, respectively, and $N$ is the number of vertical levels within the optimization layer. The smaller the RMSE, the better the stretched profiles approximate the profiles of the warm period.

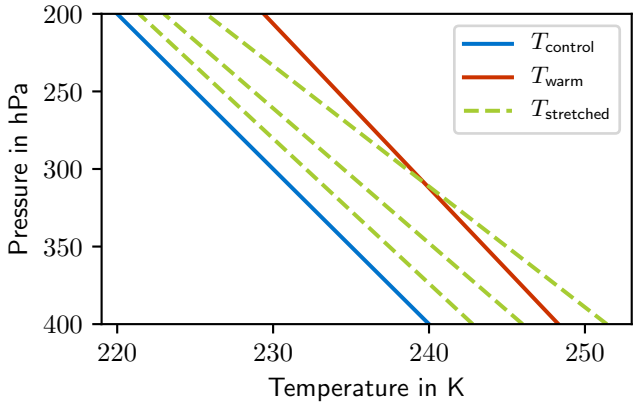


FIGURE 2.3: Illustration of the optimization method for the control temperature profile ($T_{\text{control}}$, blue line) and the warm temperature profile ($T_{\text{warm}}$, red line). The dashed green lines indicate stretched control temperature profiles ($T_{\text{stretched}}$) for different stretching parameters.

The control profiles for $T$ and $q$, which are used for the optimization of the stretching parameters $\beta_q$ and $\beta_T$, are averaged over the first 30 years as control period. The warm profiles for $T$ and $q$ are 30-year averages of the profiles in a warm period. I estimate the optimal stretching parameters with respect to the control period for 17 different warm periods. The warm periods start 5 years apart from each other. The first warm period is from year 30 to 60, the last in the end of the model run from year 110 to 140. I calculate the optimal stretching parameters $\beta_T$ and $\beta_q$ of all individual grid points in the tropics (30°N–30°S) separately.

## 2.3 Model data

To test the new perspective on long term changes in $T_B$, long time series of $T_B$, $T$ and $q$ are needed. Satellite measurements of $T_B$ are too short to investigate climatic trends. Furthermore, measurements of $T$ and $q$ profiles are rare and their temporal and spatial resolution is low. Therefore, I use model data instead.

I use 20 global coupled circulation models (Table 2.1) which are all part of the fifth phase of the Coupled Model Intercomparision Project (CMIP5, Taylor et al. (2012)). All models are driven under standardized boundary conditions to make the results comparable. I use data from the 1pctCO2 experiment (Taylor et al., 2012), where the $CO_2$ concentration increases by 1% per year to a quadrupling of the initial $CO_2$ concentration after 140 years. This induces a smooth global warming with an evolution of the $CO_2$ concentration similar to the projected $CO_2$ concentrations for the current century.

TABLE 2.1: Table of used CMIP5 models, their transient climate response (TCR, Flato et al., 2014) and the tropical average of the change in brightness temperature ($\Delta T_B$) from the control period (average over years 0–30) and the last warm period (average over years 110–140) for the 1pctCO2 run in each model, caluclated with RTTOV.

| model | TCR in K | Average $\Delta T_B$ in the tropcis |
|---|---|---|
| ACCESS1-3 | 1.7 | -0.13 |
| BCC-CSM1-1 | 1.7 | -0.25 |
| CanESM2 | 2.4 | -0.5 |
| CESM1-BGC | 1.7 | 0.05 |
| CCSM4 | 1.8 | 0.02 |
| FGOALS-g2 | 1.4 | -0.46 |
| GFDL-CM3 | 2.0 | -0.13 |
| GFDL-ESM2G | 1.1 | -0.16 |
| GFDL-ESM2M | 1.3 | -0.21 |
| GISS-E2-H | 1.7 | -0.45 |
| HadGEM-ES | 2.5 | 0.03 |
| IPSL-CM5A-LR | 2.0 | -0.27 |
| IPSL-CM5A-MR | 2.0 | -0.49 |
| IPSL-CM5B-LR | 1.5 | -0.03 |
| MIROC5 | 1.5 | -0.08 |
| MIROC-ESM | 2.2 | -0.22 |
| MPI-ESM-LR | 2.0 | -0.18 |
| MPI-ESM-MR | 2.0 | 0.04 |
| NorESM1-M | 1.4 | 0.05 |
| NorESM1-ME | 1.6 | -0.03 |

For the radiative transfer simulations with RTTOV, all model inputs are interpolated to a consistent pressure grid of 17 pressure levels between 1000 and 10 hPa. Furthermore, I only use data for the tropics between 30°N and 30°S. In Chapter 3 and 4 I show the results only for the Max Planck Institute Earth System Model (MPI-ESM, Giorgetta et al. (2013)) in low-resolution configuration (LR) in detail. Its T63L47 model grid corresponds to a horizontal resolution of approximately 1.9° and a vertical resolution of 47 levels extended to 0.01 hPa.

# Chapter 3

# Influence of vertical stretching in an idealized experiment

The goal of this thesis is to create a new perspective on $\Delta T_B$ by connecting it to a vertical stretching of the $T$ and $q$ profiles. As already mentioned in Section 2.2.1, I expect to find a correlation between the difference of both stretching parameters and $\Delta T_B$. To test if this approach is plausible, I investigate the general influence of stretching the $T$ and $q$ profiles on $\Delta T_B$ in an idealized experiment. First, I investigate the sensitivity of $\Delta T_B$ to a separate stretching of either $T$ or $q$, while the other profile remains constant. Afterwards, I investigate the sensitivity of $\Delta T_B$ to a simultaneous stretching of both profiles with independent stretching parameters for $T$ and $q$. In each case, I analyze the dependence of $\Delta T_B$ on the difference of the stretching parameters.

For the idealized experiment, the tropical average of the control period (years 0–30) in the MPI-ESM-LR is used as reference for $T$ and $q$ (Figure 3.1). In a first step, the $T$ profile remains unchanged at the control profile and the $q$ profile is stretched in 40 equal steps for $\beta_q$ in a range between 1 and 1.3. For each pair of profiles, $\Delta T_B$ is calculated with respect to $T_B$ of the control profiles. I repeat this method for an unchanged $q$ profile, stretching the $T$ profile for $\beta_T$ in 40 equal steps in a range between 1 and 1.3. From Section 2.1, I expect $\Delta T_B$ to be proportional to the difference $\beta_q - \beta_T$. I expect $\Delta T_B$ to be negative when the $q$ profile is stretched and positive when the $T$ profile is stretched.

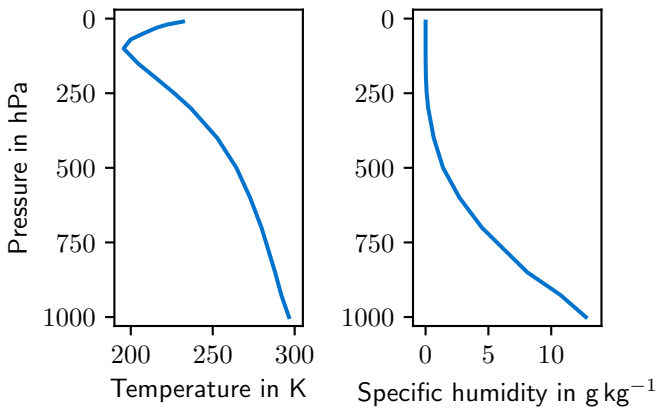


FIGURE 3.1: Control profiles for temperature $T$ (left) and specific humidity $q$ (right) for the idealized experiment.

The results of the influence on $\Delta T_B$ of stretching $T$ and $q$ separately are shown in Figure 3.2. In this case, the difference $\beta_q - \beta_T$ is positive for stretching $q$ and negative for

stretching $T$. As expected, $\Delta T_B$ is negative when the $q$ profile is stretched and positive when the $T$ profile is stretched. $\Delta T_B$ changes approximately linearly with $\beta_q - \beta_T$. Furthermore, the opposing influences of $\beta_T$ and $\beta_q$ on $\Delta T_B$ have similar amplitudes for equal stretching parameters. Thus, $\Delta T_B$ is expected to be close to zero for an equal stretching of $T$ and $q$ because their opposing influences on $\Delta T_B$ cancel out.

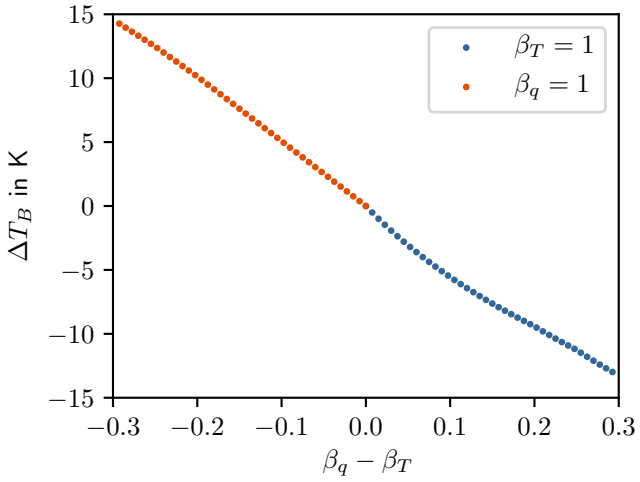


FIGURE 3.2: Change in brightness temperature ($\Delta T_B$) scattered against the difference in stretching parameters for the specific humidity and temperature profiles ($\beta_q - \beta_T$), for constant $\beta_q$ and $\beta_T$ ranging between 1 and 1.3 (red dots) and for constant $\beta_T$ and $\beta_T$ ranging between 1 and 1.3 (blue dots).

In a second step, I investigate the influence on $\Delta T_B$ of a simultaneous stretching of both profiles. To do so, I calculate $\Delta T_B$ for 1600 pairs of stretched $T$ and $q$ profiles corresponding to all possible combinations of 40 different values of $\beta_q$ and $\beta_T$ between 1 and 1.3. Again, the tropical mean profiles averaged over the control period (years 0–30) in the MPI-ESM-LR are used as the control profiles for $T$ and $q$. From my findings above I expect $\Delta T_B$ to be approximately zero for equal stretching parameters. For $\beta_q > \beta_T$ I expect $\Delta T_B$ to be positive and negative for $\beta_q < \beta_T$.

The overall behavior of $\Delta T_B$ in Figure 3.3 agrees with the results found for an individual stretching. An increase of $\beta_q - \beta_T$ corresponds to a decrease of $\Delta T_B$ and vice versa. The values of $\Delta T_B$ for $\beta_q = \beta_T$ are close to zero. Thus, $\Delta T_B$ can indeed be interpreted as a result of a vertical stretching. The lines of constant $\beta_q - \beta_T$ in Figure 3.3 are roughly parallel to lines of constant $\Delta T_B$. Furthermore, the distance of the lines of constant $\Delta T_B$ remains approximately constant. From this, I expect to find a linear relationship between the difference of the stretching parameters and $\Delta T_B$ for a simultaneous stretching of $T$ and $q$.

Figure 3.3 not only shows that the connection between $\Delta T_B$ and $\beta_q - \beta_T$ is likely to be linear, but further gives information about the expected evolution of this connection. The lines of constant $\Delta T_B$ are not exactly parallel but diverge slightly for greater stretching parameters. Thus, $\Delta T_B$ gets less sensitive to the difference $\beta_q - \beta_T$ as the climate warms and the stretching parameters increase. Therefore, I expect the slope of the linear relationship between $\Delta T_B$ and $\beta_q - \beta_T$ to decrease as the climate warms.

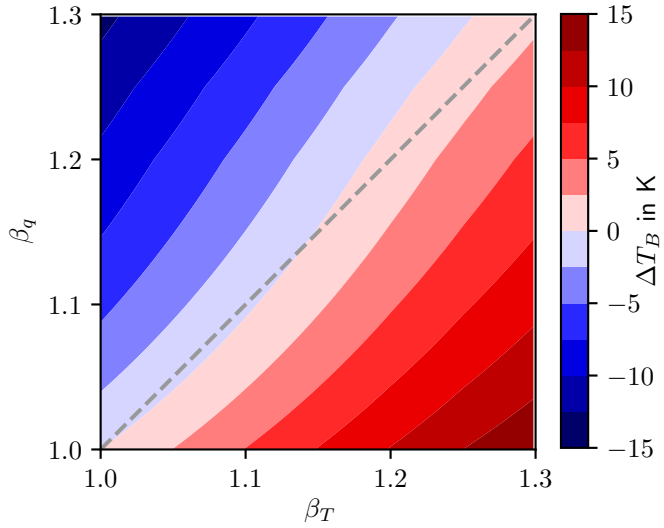


FIGURE 3.3: Dependence of the change in brightness temperature ($\Delta T_B$) on the stretching parameters $\beta_T$ for the temperature profile and $\beta_q$ for the specific humidity profile.

A reason for this decreasing sensitivity of $\Delta T_B$ on the stretching parameters could be the temperature lapse rate feedback (Manabe and Stouffer, 1980; Mokhov and Akperov, 2006). In the tropics, the temperature lapse rate, called lapse rate hereafter, is close to the moist adiabatic lapse rate due to strong convection. For increasing $T$ the moist adiabatic lapse rate decreases, and with it the actual tropical lapse rate, and the tropical mean $T$ is expected to increase more strongly in the upper troposphere than in the lower troposphere (Manabe and Stouffer, 1980; Fu et al., 2011). As illustrated in Figure 3.4, a greater shift in the emission layer is needed to reach the same $\Delta T_B$ for a weaker lapse rate. In other words, $\Delta T_B$ is less sensitive to vertical stretching for a weaker lapse rate.

Stretching the control profile of $T$ decreases the lapse rate in the upper troposphere. Thus, as the stretching parameters increase, $\Delta T_B$ gets less sensitive to their difference. Therefore, the temperature lapse rate feedback could explain the divergence of constant $\Delta T_B$ lines for increasing stretching parameters.

In Figure 3.5, all calculated values of $\Delta T_B$ for the 1600 different pairs of stretching parameters are scattered against the difference of the corresponding stretching parameters. There is indeed a strong linear relationship with a correlation coefficient below -0.99. The relationship is similar to that found in Figure 3.2. The small spread can be explained by the fact that the lines of constant $\Delta T_B$ are not perfectly straight. Therefore, the value of $\Delta T_B$ does not remain constant for a constant difference of the stretching parameters as they increase.

As expected above from Figure 3.3, there is a small dependence of the linear relationship on the value of the stretching parameters themselves (Figure 3.5). The slope of the linear relationship gets weaker as the stretching parameters increase. The linear fit for all stretched profiles has a slope of -45.9 K. For small values of $\beta_q$ and $\beta_T$ (between 1 and 1.05) the slope of the linear fit is -56.2 K and for large values of $\beta_q$ and $\beta_T$ (between 1.25 and 1.3) the slope is weaker with only -42.4 K.

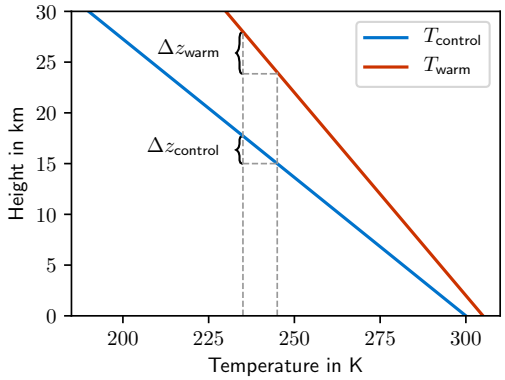


FIGURE 3.4: Illustration of the temperature lapse rate effect. The simplified control temperature profile (blue line) has a steeper lapse rate than the evolved warmer temperature profile (red line). The gray dotted lines indicate the upward shift $\Delta z_{\text{control}}$ and $\Delta z_{\text{warm}}$ which is needed for the control and warm profile, respectively, to reach the same temperature difference.

The results of this chapter show that it is possible to connect $\Delta T_B$ to a vertical stretching of a single idealized $T$ and $q$ profile. There is a strong linear relationship between the difference of the stretching parameters and $\Delta T_B$. This relationship depends to a small degree on the stretching parameters themselves. The higher the stretching parameters, the less sensitive is $\Delta T_B$ to a difference of the stretching parameters. In the next Chapter I investigate the ability of vertically stretching all individual tropical profiles to describe the corresponding $\Delta T_B$.

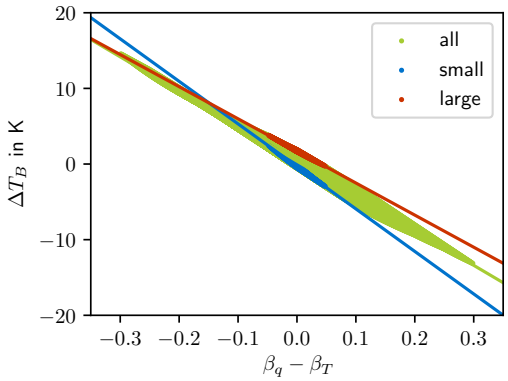


FIGURE 3.5: Dependence of the change in brightness temperature $\Delta T_B$ on the difference of the stretching parameters for specific humidity and temperature ($\beta_q - \beta_T$) for all 1600 pairs of 40 values of $\beta_q$ and $\beta_T$ between 1 and 1.3, respectively (green dots), small values of $\beta_q$ and $\beta_T$ between 1 and 1.05 (blue dots) and large values of $\beta_q$ and $\beta_T$ between 1.25 and 1.3 (red dots) and the respective linear fits (solid lines).

# Chapter 4

# The new perspective in coupled climate models

The results in Chapter 3 show that for an idealized experiment, there is a strong correlation between $\Delta T_B$ and the difference of the stretching parameters. Thus, the new perspective on $\Delta T_B$ is applicable to this idealized case. In this Chapter I test the applicability of the new perspective to coupled climate models which simulate a more complex evolution of the $T$ and $q$ profiles in a warming climate, which might differ from a simple vertical stretching.

In Section 4.1 I investigate the ability of vertical stretching to describe the profiles' evolution in a warming scenario in the MPI-ESM-LR, first for the tropical mean and then for all individual tropical profiles. In Section 4.2 I test the new perspective on $\Delta T_B$, again for data from the MPI-ESM-LR. Finally, I extend the analysis to 19 further models from the CMIP5 ensemble in Section 4.3 to test the new perspective on its robustness across several climate models.

## 4.1 Vertical stretching in the MPI-ESM-LR

The main assumption of the new perspective on $\Delta T_B$ is that stretching the $T$ and $q$ profiles is able to describe the actual evolution of the tropical profiles in a warming climate. In this section I give an overview of the distribution of the optimized stretching parameters $\beta_q$ and $\beta_T$ in the tropics and the ability of vertical stretching to represent the profiles' evolution in a warming climate in the MPI-ESM-LR.

The stretched profiles correspond to the control profiles (average over years 0–30) for all tropical grid cells, stretched by their optimal stretching parameters using the Equations 2.2 and 2.1. I optimize the stretching parameters as described in Section 2.2.2, by minimizing the RMSE between the stretched profiles and the 30-year mean profiles for the 17 different warm periods. I calculate the optimal stretching parameters for all individual tropical profiles for $T$ and $q$ separately. In this section I compare the stretched profiles to the warm profiles which should be approximated by the vertical stretching. All results are shown for the last warm period (years 110–140).

### 4.1.1 Tropical average

Before I look at the individual profiles in the MPI-ESM-LR, I first investigate the ability of the tropical mean of all stretched $T$ and $q$ profiles to describe the tropical mean of the actual profiles' evolution in this section.

After stretching the profiles separately, I average the stretched profiles over the tropics and compare the mean stretched $T$ and $q$ profiles to the tropical mean profiles of the last warm period. Note that the average of the stretched profiles is not exactly equal, albeit very similar, to stretching the tropical mean control profile by the mean stretching parameters. For the last warm period, the tropical mean values for the stretching parameters are $\beta_q = 1.164$ and $\beta_T = 1.156$.

The mean stretched profiles of $T$ and $q$ match well with the tropical mean profiles of the last warm period (Figure 4.1a and b) within the optimization layer for the stretching parameters (400–200 hPa). The RMSE between the mean stretched profiles and the warm profiles is small with values of 0.018 g kg$^{-1}$ for $q$ and 0.85 K for $T$ within the optimization level.

However, for the new perspective it is not only the profile itself which has to fulfill the assumption of stretching as a good approximation. Rather, it is the difference between the stretched profile and the control profile which has to fit with the difference of the warm profile and the control profile to represent the profiles' evolution in a warming climate. To account for this, I normalize the absolute errors of $T$ and $q$ by the difference in the warm and the control profiles to obtain the relative error:

$$E_{\text{rel}} = \frac{x_{\text{stretched}} - x_{\text{warm}}}{x_{\text{warm}} - x_{\text{control}}}, \tag{4.1}$$

where $x_{\text{stretched}}$, $x_{\text{warm}}$ and $x_{\text{warm}}$ are values for either $q$ or $T$ of the stretched, the warm and the control profile, respectively.

For the optimized layer, the relative error is below 14% for $\Delta q$ and below 10% for $\Delta T$ (Figure 4.1c). For levels below and above the optimization layer, the relative error increases. However, these layers are not primarily important for $\Delta T_B$ because most of the signal comes from the optimization layer. Thus, it can be concluded that for the tropical average, stretching the $T$ and $q$ profiles is a good approximation of the profiles' evolution in the MPI-ESM-LR.

### 4.1.2 Individual profiles

Above I showed that averaged over the tropics, vertical stretching is a good approximation of the actual profiles' evolution. In this section I take a more detailed look at the profiles in the individual grid cells of the MPI-ESM-LR. First, I analyze the distribution and range of the optimal stretching parameters which were calculated in Section 4.1.1 for all individual tropical profiles. Then, I investigate the ability of vertical stretching to describe the actual evolution of these individual profiles. Furthermore, I analyze the distribution of the relative error between the vertically stretched profiles and the warm profiles in the optimization layer (400–200 hPa).

The tropical temperature distribution in the upper troposphere is very homogeneous (Bretherton, 2000). Similarly, the distribution of $\beta_T$ is homogeneous over the tropics with slightly increasing values towards the equator (Figure 4.2a). This matches with regions, where the temperature change is strongest within the optimization layer (Figure A.2). The spatial variance of $\beta_T$ for one warm period is much smaller than the change of its tropical mean over time.

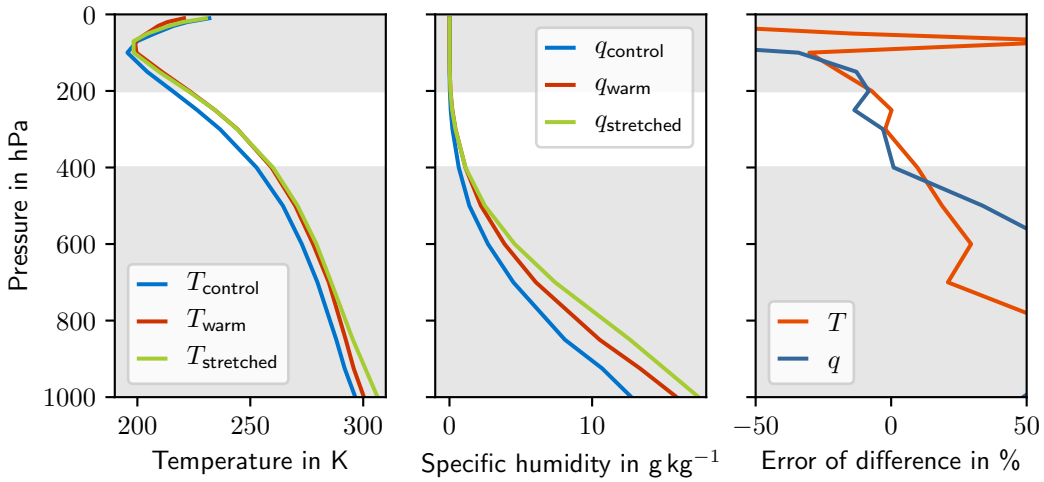


FIGURE 4.1: Tropical mean of the control profile (blue), warm profile (red) for the last warm period (years 110–140) and stretched profile (green) for the temperature $T$ (left panel) and specific humidity $q$ (center panel) as well as the relative error of the stretched profile to the warm profile (right panel) normalized by the difference between the warm and the control profile for $T$ (red) and $q$ (blue).

In contrast to $\beta_T$, the distribution of $\beta_q$ is inhomogeneous (Figure 4.2b) and its spatial variance of $\beta_q$ is much higher than the change of its tropical mean over time. The largest values of $\beta_q$ are located in the subsidence zones over the East Pacific, over the Arabian Sea and in the ITCZ (Inter Tropical Convergence Zone) regions over the Pacific. These regions roughly match with the regions of the strongest surface warming over the ocean (Figure A.7b). The range of $\beta_q$ is smaller for profiles over land than for profiles over the ocean even though the changes in the near-surface temperature are largest over land (A.7b). The reason for this is likely the limited water availability over land (Byrne and O'Gorman, 2013) which not only causes the amount of near-surface specific humidity to be less over land (Figure A.7c), but further reduces the increase in near-surface specific humidity in a warming climate (Figure A.7d).

Even though the spatial distribution and variance of $\beta_T$ and $\beta_q$ differ, the tropical averages of both stretching parameters develop similarly (Figure A.1). Both stretching parameters increase by approximately 0.7% between two warm periods with a stronger increase for later warm periods. As already mentioned in Section 4.1.1, for the last warm period the mean values of the stretching parameters are $\beta_T \approx 1.156$ and $\beta_q \approx 1.164$.

The comparison of the individual $T$ profiles of the warmer climate to the stretched control profiles shows that stretching the $T$ profiles is a good assumption, not only for the tropical average, but also for all individual profiles. The relative error of stretching $T$, normalized with the actual change $\Delta T$, is below 7% for 90% of all tropical profiles (Figure 4.2c) within the optimization layer. The RMSE between the stretched $T$ profiles and the warm $T$ profiles is below 2 K in general and even below 1 K for most tropical profiles (Figure A.8a). The error is homogeneous in the deep tropics and reaches the highest values in the subtropics.

Similar to the T profiles, stretching the q profiles is a good approximation for the evolution of most individual tropical $q$ profiles, as the relative error for $\Delta q$ is below 18% for 90%

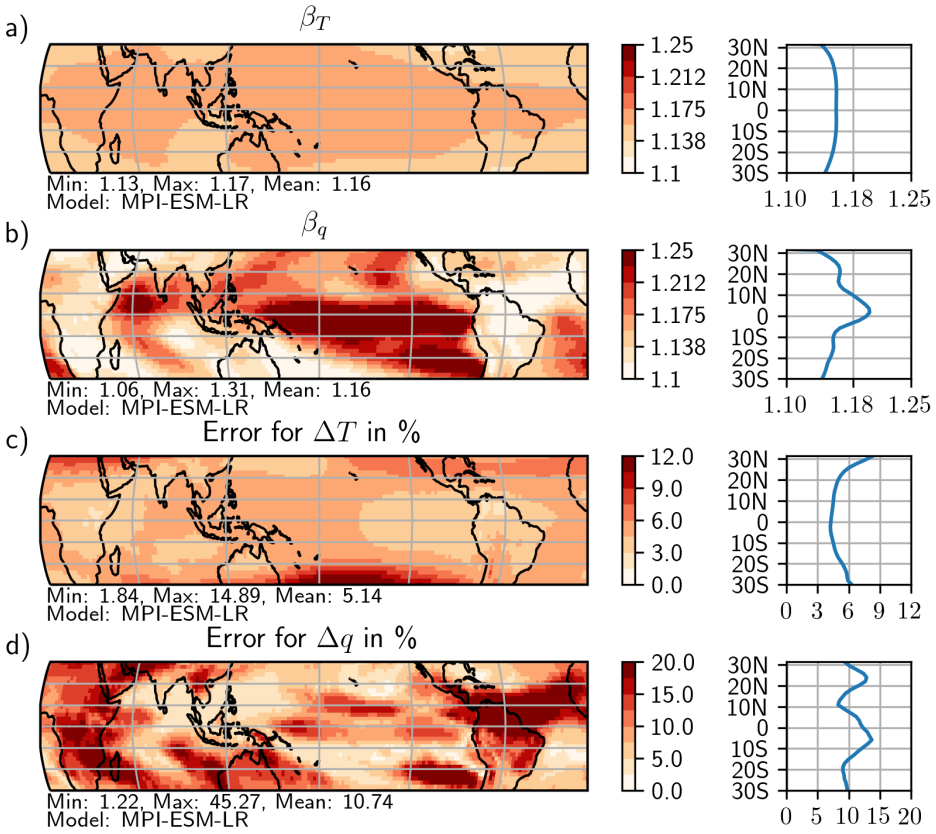


FIGURE 4.2: Optimal stretching parameters for temperature (a) and specific humidity (b) as well as the relative error of the stretched profiles to the warm profiles, normalized by the difference between the warm and the control profiles for the change in temperature (c) and the change in specific humidity (d).

of all tropical profiles (Figure 4.2d) within the optimization layer. The RMSE is below 0.05 g kg$^{-1}$ for most of the profiles (Figure A.8b). Over land the error for $\Delta q$ is the largest. Apart from that, the error is particularly high in the ITCZ region over the Atlantic and Pacific, the El Niño region and the region of the Indian and Australian Monsoon circulation systems. As already mentioned by Singh and O'Gorman (2012), vertically stretching is able to capture the vertical changes in the troposphere but not necessarily the horizontal changes. Therefore, I suspect the evolution of the profiles in these regions to deviate from a pure vertical stretching due to various additional impacts. Such impacts could be a potential weakening of the Walker (Plesca et al., 2018; Sohn et al., 2019) and Hadley circulations (Lau and Kim, 2015), a changing intensity (Stevenson, 2012; Kim and Yu, 2012) or frequency of the the El Niño phenomenon (not projected for MPI-ESM-LR; Cai et al. (2014)), a narrowing (Byrne and Schneider, 2016) or weakening of the ITCZ (Byrne et al., 2018) and a shift and change in intensity of the Monsoon systems (Hsu et al., 2012; Wang et al., 2014). Still, the errors in these regions are small and thus vertical stretching is able to describe the evolution of most individual tropical $q$ profiles.

From the results of this section it can be concluded that vertically stretching is able to describe most of the changes in the optimization layer, which corresponds approximately to the emission layer of $T_B$ for water vapor channels. Therefore, vertical stretching is a suitable simplification for investigations on $\Delta T_B$ in a warming climate.

## 4.2 The new perspective in the MPI-ESM-LR

In Chapter 3 I showed for an idealized experiment that changes in $T_B$ are connected to a vertical stretching of the $T$ and $q$ profiles. Furthermore, I showed above that the simplification of vertical stretching is able to describe the major profile changes in the MPI-ESM-LR. In this section, I show that this opens a new perspective on $\Delta T_B$ which is also applicable for model data from the MPI-ESM-LR and test if the results for the model match with the results from the idealized experiment in Chapter 3. First, I analyze the distribution of $\Delta T_B$ in the MPI-ESM-LR and compare it to the distribution of the stretching parameters. Second, I apply the new perspective on $\Delta T_B$ to the MPI-ESM-LR by connecting $\Delta T_B$ to the difference of the stretching parameters. Finally, I compare the results to the idealized experiment.

In the MPI-ESM-LR the tropical mean of $\Delta T_B$ is slightly negative for all warm periods. The largest difference to the control period appears in the last warm period with $\Delta T_B \approx -0.18\,\mathrm{K}$. In comparison, the local values of $\Delta T_B$ are in the order of 10 times larger (Figure 4.3) and the spatial distribution of $\Delta T_B$ is inhomogeneous. The largest negative changes in $T_B$ are located over the East and Middle Pacific, the Arabian Sea and the South Atlantic Ocean. The largest positive values of $\Delta T_B$ are located over Oceania, Madagascar, South America and over the Atlantic ITCZ region.

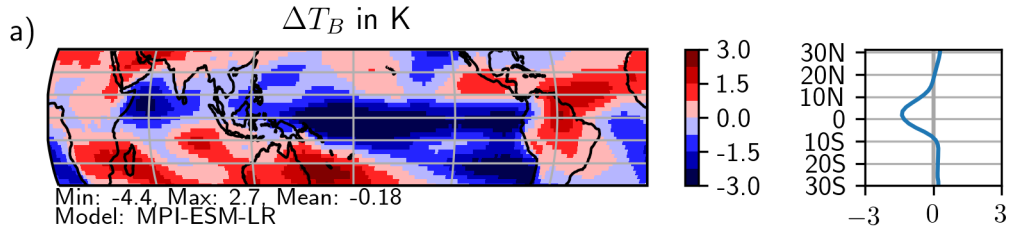


FIGURE 4.3: Change in brightness temperature in the MPI-ESM-LR, simulated for AMSU-B ($183.31 \pm 1\,\mathrm{GHz}$) between the control period (averaged over years 0–30) to the last warm period (averaged over years 110–140) as well as its zonal average (right sub-panel).

When comparing the regional distribution of $\Delta T_B$ to the distribution of the stretching parameters, the overall patterns of $\Delta T_B$ match notably well with the patterns of $\beta_q$. This is an indication that the new perspective is also applicable for the MPI-ESM-LR. Furthermore, I expect the connection of $\Delta T_B$ to the stretching parameters to be mostly driven by $\beta_q$ because $\beta_T$ is homogeneous over the tropics. Therefore, even though the connection in the idealized experiment shows that $\Delta T_B$ depends on the difference of both stretching parameters, I expect $\beta_q$ to be the crucial parameter determining the distribution of $\Delta T_B$ in the model with only a slight dependence on $\beta_T$.

Applying the new perspective to the MPI-ESM-LR, there is indeed a strong linear dependence of $\Delta T_B$ on the difference of the optimized stretching parameters for $T$ and $q$ (Figure 4.4a). The correlation is below $-0.84$ for all 17 warm periods and even below $-0.9$ for later warm periods (Table 4.1). Thus, the new perspective on $\Delta T_B$ is also applicable for the individual tropical profiles from the MPI-ESM-LR.

The relationship between $\Delta T_B$ and $\beta_q - \beta_T$ for the individual profiles of the MPI-ESM-LR changes similarly to the idealized experiment in Chapter 3. As in the idealized case

TABLE 4.1: Table of the parameters for the linear relationship between $\Delta T_B$ and $\beta_q - \beta_T$ and its correlation for all 17 warm periods in the MPI-ESM-LR. A linear relationship is described by the slope $m$ and the intercept $b$.

| Warm period | Year | $m$ in K | $b$ in K | Correlation coefficient |
|---|---|---|---|---|
| 1 | 30-60 | −37.46 | −0.22 | −0.86 |
| 2 | 35-65 | −34.97 | −0.23 | −0.86 |
| 3 | 40-70 | −30.91 | −0.21 | −0.85 |
| 4 | 45-75 | −31.36 | −0.24 | −0.85 |
| 5 | 50-80 | −30.81 | −0.27 | −0.85 |
| 6 | 55-85 | −31.29 | −0.26 | −0.84 |
| 7 | 60-90 | −30.83 | −0.27 | −0.86 |
| 8 | 65-95 | −30.03 | −0.26 | −0.86 |
| 9 | 70-100 | −30.83 | −0.28 | −0.86 |
| 10 | 75-105 | −28.04 | −0.22 | −0.89 |
| 11 | 80-110 | −27.36 | −0.19 | −0.90 |
| 12 | 85-115 | −27.01 | −0.17 | −0.90 |
| 13 | 90-120 | −25.86 | −0.12 | −0.92 |
| 14 | 95-125 | −24.90 | −0.06 | −0.93 |
| 15 | 100-130 | −25.47 | −0.03 | −0.93 |
| 16 | 105-135 | −25.54 | 0.01 | −0.94 |
| 17 | 110–140 | −25.72 | 0.03 | −0.94 |

(Figure 3.5), for increasing stretching parameters the slope is decreasing (Figure 4.4b, Table 4.1). The suspected reason for this decrease in sensitivity of $\Delta T_B$ on vertical stretching is a decrease of the lapse rate within the emission layer as the climate warms, as described in Chapter 3.

These similarities are also evident in the dependence of $\Delta T_B$ on the individual stretching parameters (Figure 4.5a). As in the idealized experiment (Figure 4.5b), $\Delta T_B$ is mostly positive for $\beta_q < \beta_T$ and mostly negative for $\beta_q > \beta_T$, even though $\Delta T_B$ is less sensitive on the stretching parameters. For $\beta_q = \beta_T$ the values of $\Delta T_B$ are close to zero. Similar to the idealized experiment, equal stretching corresponds to a slightly negative $\Delta T_B$ for small stretching parameters which increases for larger stretching parameters.

A more detailed analysis of the connection of $\Delta T_B$ to the stretching parameters reveals some differences between the model data and the idealized experiment. The slope of the dependence of $\Delta T_B$ is generally weaker for the MPI-ESM-LR than for the idealized case (Figure 3.5) for all 17 warm periods. Part of the reason is that the range of the appearing stretching parameters in the model differs from the range of the stretching parameters used in the idealized experiment. Repeating the idealized experiment using only pairs of $\beta_q$ and $\beta_T$ which occur in the model, slightly reduces the slope of the connection between $\Delta T_B$ and $\beta_q - \beta_T$ (Figure A.4).

Another probably more important reason for this difference might be other atmospheric processes which are not captured by a vertical stretching and additionally influence $\Delta T_B$. When comparing the actual $\Delta T_B$ to $\Delta T_B$ resulting from vertically stretched profiles (Figure 4.6), the actual change is much weaker. Thus, there must be additional influences

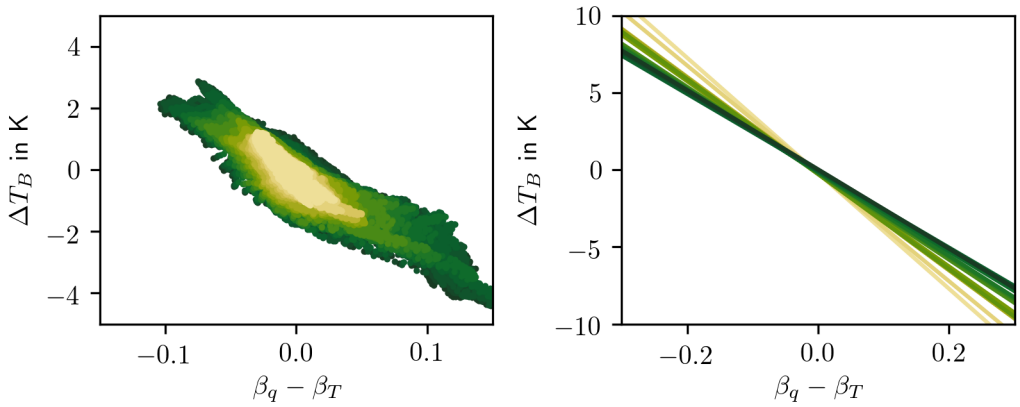


FIGURE 4.4: Change in brightness temperature ($\Delta T_B$) as a function of the difference of the optimal stretching parameters for the specific humidity and temperature $\beta_q - \beta_T$ (left panel) and the corresponding linear fits (right panel) for all 17 warm periods between the years 30–60 (beige line) and the years 100–140 (dark green line).

on $\Delta T_B$ which are not captured by the vertical stretching. One of these additional influences might be that actual change in the lapse rate is slightly underestimated (Singh and O'Gorman (2012), their Figure 7b and 10b)

Regardless of the difference in the slope, there is still a high correlation between $\Delta T_B$ for the model and for the stretched profiles as well as between $\Delta T_B$ and $\beta_q - \beta_T$. This shows that the additional processes produce systematic differences in $\Delta T_B$. Nevertheless, the new perspective is applicable to model data, even though it has to be kept in mind although there are differences between the idealized experiment and the profiles' evolution in the model.

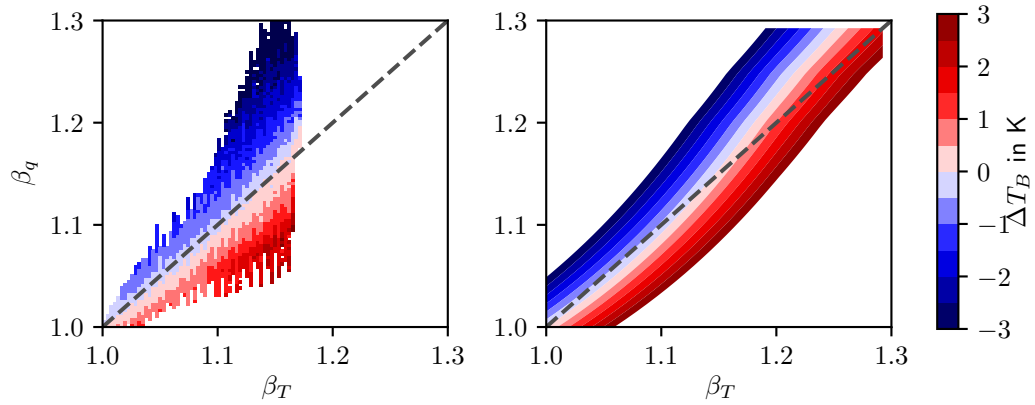


FIGURE 4.5: Dependence of the change in the simulated brightness temperatures ($\Delta T_B$) on the optimal stretching parameters $\beta_T$ and $\beta_q$ for the temperature and specific humidity profiles in all 17 warm periods for all tropical profiles in the MPI-ESM-LR (left panel) and for the profiles of the idealized experiment in Chapter 3 (right panel).

## 4.3 Robustness of the new perspective across the CMIP5 ensemble

In the previous Section I showed that the new perspective of $\Delta T_B$ is applicable for the CMIP5 model MPI-ESM-LR. However, even if all CMIP5 models are driven by the same external forcing, they differ remarkably in some of their results for the climate sensitivity and the upper tropospheric water vapor (Jiang et al., 2012; John and Soden, 2007). These differences lead in turn to different results for the simulated $\Delta T_B$ (Figure 4.7a). To test if the new perspective is applicable for different models and if there are noticeable differences in the results for the new perspective, I repeat the methods from Section 4.2 for 19 further available CMIP5 models.

First, I calculate the optimized stretching parameters $\beta_q$ and $\beta_T$ for all models and compare the tropical mean, distribution and ranges of the stretching parameters. Then, I show that in all used models, $\Delta T_B$ is connected to the difference of the stretching parameters of $T$ and $q$ and that thus the new perspective on $\Delta T_B$ is applicable. Finally, I focus on differences between the models in their relationship between $\Delta T_B$ and the stretching parameters and connect those differences to the transient climate response of each model.

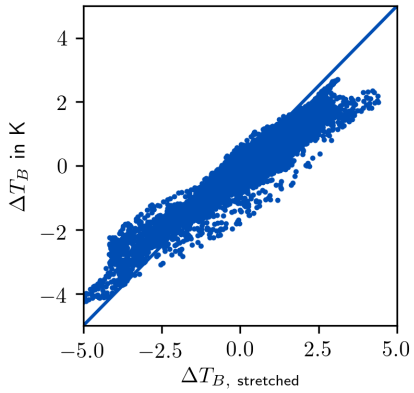


FIGURE 4.6: Change in brightness temperature ($\Delta T_B$) for all tropical grid cells in the MPI-ESM-LR scattered against the change in brightness temperature simulated for the stretched profiles between the control period (years 0–30) and the last warm period (years 110–140).

The tropical means of both stretching parameters develop similarly for every model (Figure 4.7b). Even though the range of $\beta_q$ and $\beta_T$ differs over all models, their difference $\beta_q - \beta_T$ is close to zero over the whole time series. For most of the models, $\beta_T$ increases slightly stronger in the first warm periods and is overtaken by $\beta_q$ in the latest warm periods. In line with the small difference of the stretching parameters, $\Delta T_B$ is also rather small with mostly negative changes of less than $-0.5$ K for all models (Figure 4.7a, Table 2.1).

For the individual profiles of all models, the spatial distribution of $\beta_T$ is homogeneous (Figure A.5), whereas the spatial distribution of $\beta_q$ is inhomogeneous (Figure A.6), similar to the MPI-ESM-LR. However, the patterns of $\beta_q$ are rather different for all models. The only similarity in the distribution of $\beta_q$ is that for most models $\beta_q$ reaches a maximum at the equator over the Pacific and for some models over the Arabian Sea.

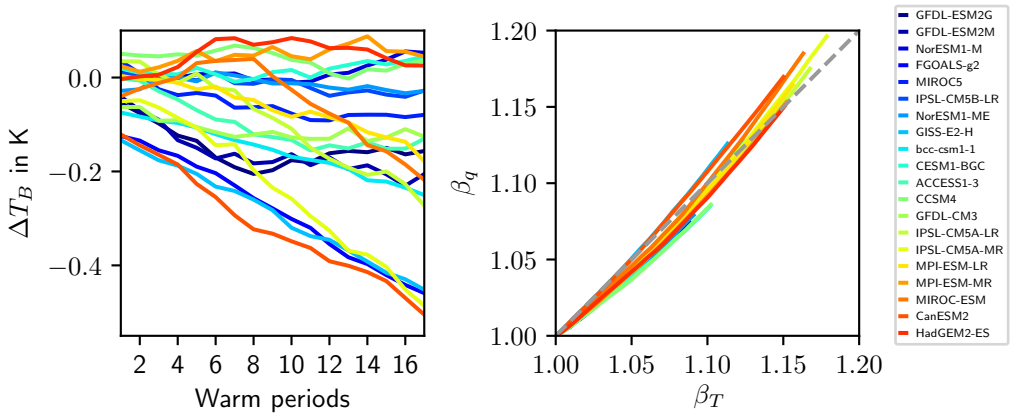


FIGURE 4.7: Evolution over all 17 warm periods of the tropical mean of the change in brightness temperature ($\Delta T_B$) (left panel) and the tropical mean of the optimal stretching parameters for temperature ($\beta_T$) and specific humidity ($\beta_q$) (right panel) for 20 different CMIP5 models.

Although the range and distribution of the stretching parameters differs strongly over all CMIP5 models, there is a strong connection between $\Delta T_B$ and the difference of the stretching parameters for each model (Figure 4.8). Thus, the new perspective on $\Delta T_B$ is applicable to every used CMIP5 model, even though the simulated $\Delta T_B$ and the stretching parameters differ across the models. The correlation coefficient between $\Delta T_B$ and the difference of the stretching parameters is below $-0.7$ in all 17 warm periods for all models. For the last warm period the correlation is stronger, below $-0.8$ for almost all models and for some even below $-0.9$.

Even though the new perspective on $\Delta T_B$ is applicable to every tested model, there are some noticeable differences in the relationship between $\Delta T_B$ and $\beta_q - \beta_T$ across the models (Figure 4.8). The slope of the relationship for the last warm period differs strongly over all models (Figure 4.8). Furthermore, the slope of the linear relationship decreases with increasing stretching parameters but the decrease differs for all models (Figure 4.9).

Models with rather small values of $\Delta T_B$ and $\beta_q - \beta_T$ tend to have steeper slopes and weaker changes of the slopes than models with greater ranges for $\Delta T_B$ and $\beta_q - \beta_T$ (shown for the last warm period in Figure 4.8). The range of the difference of the stretching parameters $\beta_q - \beta_T$ depends on the range of the individual stretching parameters $\beta_q$ and $\beta_T$ themselves. Smaller stretching parameters also result in a smaller difference of the stretching parameters. Therefore, models with stronger increases in $\beta_q$ and $\beta_T$ show stronger changes in the slope than models with weaker increases in $\beta_q$ and $\beta_T$. This is in line with the expectations in Chapter 3 that $\Delta T_B$ gets less sensitive to stretching with increasing stretching parameters.

The suspected reason for these differences in the slopes (Figure 4.9) is that the sensitivity of $\Delta T_B$ to stretching depends on the temperature lapse rate. As the stretching parameters increase, the temperature lapse rate decreases. This results in a decreasing sensitivity of $\Delta T_B$ on vertical stretching because the same shift of the emission layer leads to a smaller change in $T_B$ for a steeper temperature lapse rate (see Chapter 3).

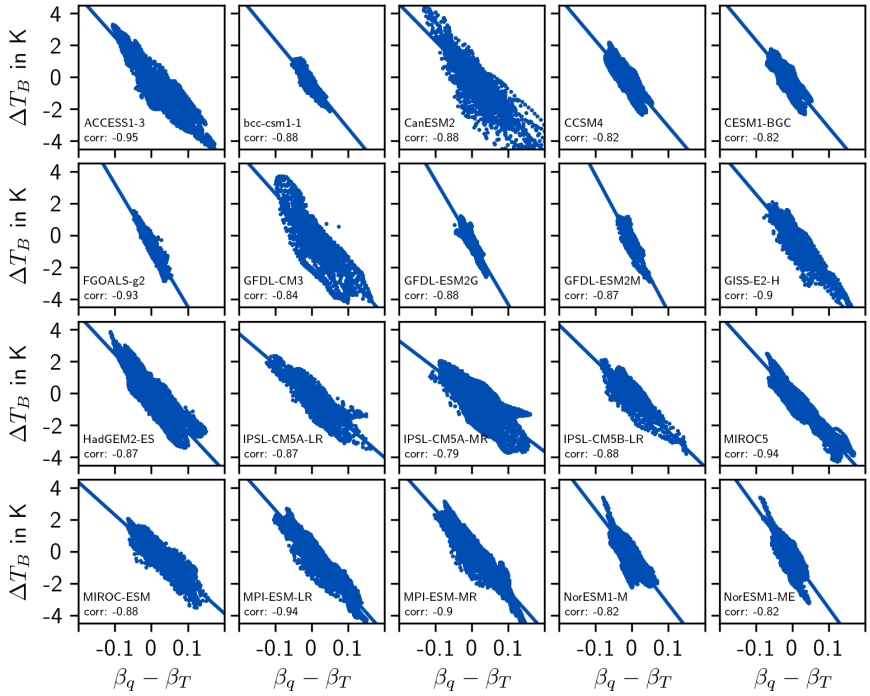


FIGURE 4.8: Change in brightness temperature ($\Delta T_B$) for all tropical grid cells as a function of the difference of stretching parameters $\beta_q - \beta_T$ (dots) and the corresponding linear fit (line) for the last warm period (years 110–140) for 20 different CMIP5 models.

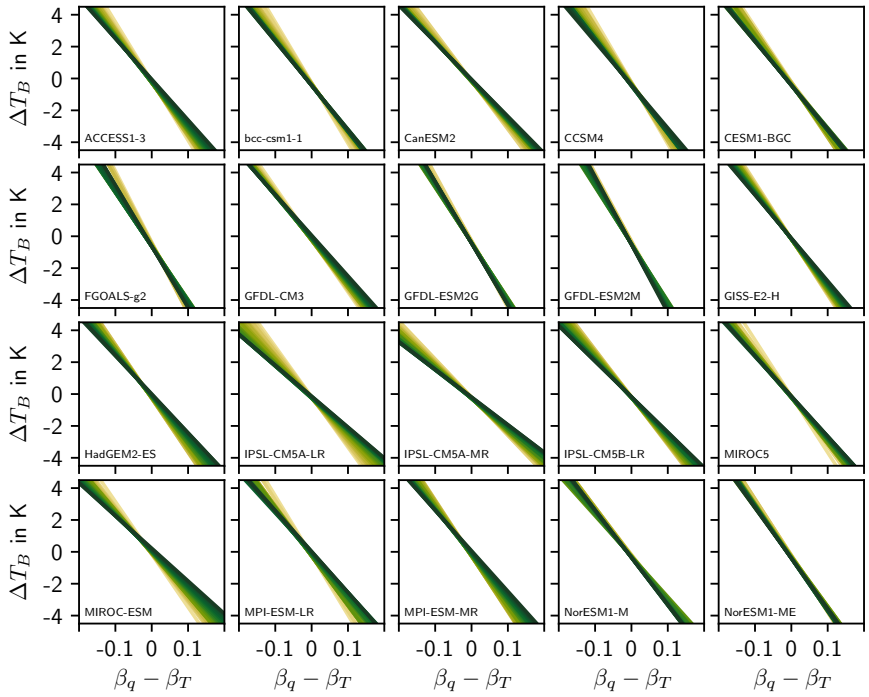


FIGURE 4.9: Linear relationship between the change in brightness temperature ($\Delta T_B$) and the difference of stretching parameters ($\beta_q - \beta_T$) for all 17 warm periods between the years 30–60 (beige lines) and the years 100–140 (dark green lines) for all used CMIP5 models.

A further investigation of the differences reveals that the slope of the linear relationship between $\Delta T_B$ and $\beta_q - \beta_T$ correlates with the transient climate response (TCR) of the individual models (Figure 4.10, Table 2.1). The TCR is defined as the change in global and annual mean surface temperature in the 1pctCO2 run and calculated using the difference between the start of the experiment and a 20-year period centered on the time of $CO_2$ doubling (Flato et al., 2014). The TCR is a good indicator of the influence of an increase in $CO_2$ on the temperature profiles in the tropics. Models with a weaker increase of the stretching parameters within the model run correspond to a weaker increase of the surface temperature and thus to a smaller TCR. Thus, models with a steeper slope tend to have a smaller TCR.

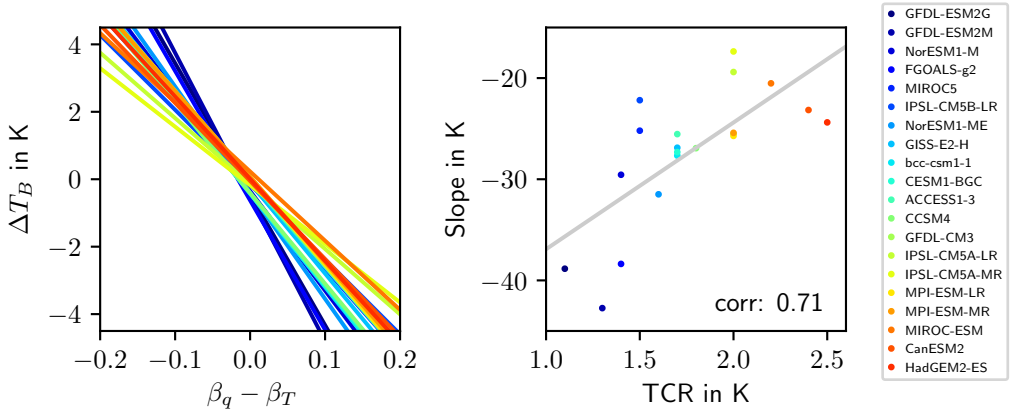


FIGURE 4.10: Linear relationship between the change in brightness temperature ($\Delta T_B$) and the difference of stretching parameters ($\beta_q - \beta_T$) for the last warm period (years 110–140) (left panel) for all models and the corresponding slopes scattered against the transient climate response (TCR) of the respective model.

In this section the new perspective was tested on its robustness over 20 CMIP5 models. The models differ in the evolution of $\Delta T_B$ as well as in the spatial distribution and temporal evolution of the stretching parameters. Nevertheless, I find a strong correlation between $\Delta T_B$ and the difference of the stretching parameters $\beta_q - \beta_T$ in all models. Therefore, the new perspective is applicable for all used CMIP5 models. This gives confidence that the new perspective might open new applications for satellite measurements. The slope of the relationship between $\Delta T_B$ and $\beta_q - \beta_T$ depends on the values of $\beta_q$ and $\beta_T$ themselves. The suspected reason for this is a decreasing sensitivity of $\Delta T_B$ on stretching due to a decrease in the temperature lapse rate. The magnitude of the slope's change within the model run differs for individual models and correlates with its climate sensitivity represented by the TCR.

# Chapter 5

# Dependence on the measurement instrument

In the previous chapter I showed that the new perspective on $\Delta T_B$ is robust for all used CMIP5 models. This gives confidence that the new perspective could also be applied to other satellite measurements. As already mentioned in Section 2.1, there are two frequency ranges that are most sensitive to changes in the upper tropospheric humidity. One frequency range lies in the microwave range and the other in the infrared range. In this thesis $\Delta T_B$ was calculated for the microwave radiometer AMSU-B for the water vapor channel 18 which is located at $183.31 \pm 1$ GHz (Section 2.1).

A recent study by Lang (2019) shows a dependence of $\Delta T_B$ on the measurement instrument for AMSU-B and the infrared radiometer HIRS. Lang (2019) suspects the cause of this dependence in the different radiometric properties of both instruments (Lang (2019), her Figure 4.3). The absorption lines are subject to the so-called pressure broadening effect (Baranger, 1958), which increases the thickness in the flanks of absorption lines for higher pressures. As a result, radiation at frequencies in the flanks is absorbed more efficiently on its way up to the top of atmosphere and a larger part of the received signal comes from higher altitudes.

In a warming climate, the emission layer of $T_B$ shifts up to lower pressures and the pressure broadening effect on the absorption lines is reduced. Thus, a larger amount of the signal of $T_B$ comes from lower, warmer parts of the emission layer. The sensitivity of $T_B$ on the reduced pressure broadening depends on the frequency range. The water vapor channel of AMSU-B lies in a frequency range close to the peak of the 183.31 GHz absorption line and is thus only slightly affected by the reduced pressure broadening. In contrast, HIRS measures in a broad absorption band around 6.7 $\mu$m including many absorption lines and their overlapping flanks. These overlapping flanks are highly affected by the reduced pressure broadening. Because of this, as the emission layer shifts upwards and the pressure broadening weakens, the measured $\Delta T_B$ is more positive for HIRS than for AMSU-B.

To make the new perspective applicable to satellite measurements, it is necessary to investigate the effect of using different measurement instruments on the relationship between $\Delta T_B$ and $\beta_q - \beta_T$. In this chapter, I analyze this difference for HIRS and AMSU-B. To do so, I repeat the idealized experiment from Chapter 3 for HIRS and compare the dependence of $\Delta T_B$ on $\beta_q - \beta_T$ to AMSU-B for data from the MPI-ESM-LR.

Before investigating the impact of using HIRS instead of AMSU-B on the results from Chapter 3 in detail, I want to roughly portray what differences I expect for HIRS. Figure 5.1 summarizes my expectations. Keeping $\beta_q$ constant and only stretching the $T$ profile (Figure 5.1a), the emission layer remains at the same height and the effect of

pressure broadening does not change. Therefore, I do not expect any differences for the dependence of $\Delta T_B$ on $\beta_T$ as both instruments should measure in similar layers in the upper troposphere.

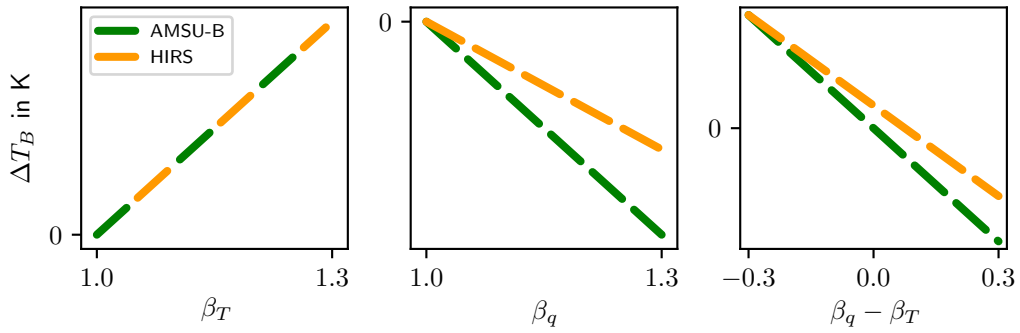


FIGURE 5.1: Illustration of the expected qualitative relationship between the change in brightness temperature ($\Delta T_B$) and the stretching parameter for the temperature profile ($\beta_T$) for setting the stretching parameter for the humidity profile ($\beta_q$) to one (left panel), between $\Delta T_B$ and $\beta_q$ for $\beta_T = 1$ (center panel) and between $\Delta T_B$ and $\beta_q - \beta_T$ (right panel) for AMSU-B (dashed green lines) and HIRS (dashed oranges lines).

Keeping $\beta_T$ constant and stretching the $q$ profile (Figure 5.1b), the dependence of $\Delta T_B$ on $\beta_q$ should differ for both instruments, as the upward shift of the emission layer to lower pressures changes the weighting of $T$ within the emission layer differently. Because mainly HIRS is affected by the reduced pressure broadening, I expect the decrease of $\Delta T_B$ with increasing $\beta_q$ to be weaker for HIRS than for AMSU-B for constant $\beta_T$.

As a consequence of the expected dependence of $\Delta T_B$ on $\beta_q$ and $\beta_T$ from above, the resulting dependence on $\beta_q - \beta_T$ should be weaker for HIRS than for AMSU-B (Figure 5.1). For increasing $\beta_T$ the dependence of $\Delta T_B$ should be equal for both instruments but the decrease of $\Delta T_B$ for an increase of $\beta_q$ should be reduced for HIRS. Together, this would lead to a weaker decrease, and thus a weaker dependence of $\Delta T_B$, as the difference $\beta_q - \beta_T$ increases. Therefore, I expect $\Delta T_B$ to be less negative for HIRS for $\beta_q > 1$.

I investigate the difference of the relationship between $\Delta T_B$ and the stretching parameters for HIRS and AMSU-B by simulating $T_B$ for both instruments using RTTOV. $\Delta T_B$ is calculated for the same profile data I used in the idealized experiment in Chapter 3. The data consists of all 1600 possible combinations of stretched $T$ and $q$ profiles, corresponding to 40 different values of $\beta_q$ and $\beta_T$ between 1 and 1.3. The control profiles of $T$ and $q$ are the tropical mean profiles averaged over the control period (year 0–30) of the MPI-ESM-LR.

Figure 5.2 shows the dependence of $\Delta T_B$ on both stretching parameters (Figure 5.2a, b) and on their difference (Figure 5.2c). The dependence of $\Delta T_B$ on $\beta_T$ is weaker for HIRS than for AMSU-B. This was not expected because the emission layer is not shifted or changed in shape. The reason for this are slightly different weighting functions within the emission layer of $T_B$ for HIRS and AMSU-B (John et al., 2011). If the lapse rate changes, this will lead to a difference in $\Delta T_B$.

The dependence of $\Delta T_B$ on $\beta_q$ (Figure 5.2b) is much weaker for HIRS. This is in line with the suspicion that the water vapor channel of HIRS is much more sensitive to the reduced pressure broadening effect, while AMSU-B remains largely unaffected. For HIRS,

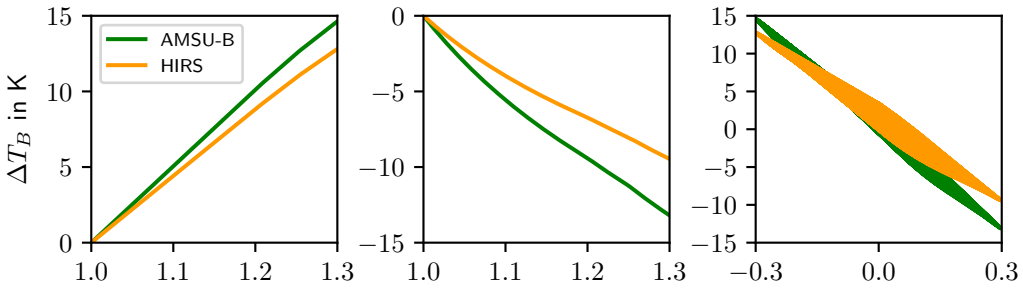


FIGURE 5.2: Relationship between the change in brightness temperature ($\Delta T_B$) and the stretching parameter for the temperature profile ($\beta_T$) for setting the stretching parameter for the humidity profile ($\beta_q$) to one (left panel), between $\Delta T_B$ and $\beta_q$ for $\beta_T = 1$ (center panel) and between $\Delta T_B$ and $\beta_q - \beta_T$ (right panel) for AMSU-B (dashed green lines) and HIRS (dashed oranges lines). The brightness temperatures are simulated for idealized profiles from Chapter 3 for the MPI-ESM-LR.

the shift of the emission layer to lower pressures changes the weighting function within the emission layer so that more signal for $\Delta T_B$ comes from lower levels. Therefore, the decrease in $\Delta T_B$ is weaker for an increase in $\beta_q$ and an upward shift of the emission layer to lower pressures and lower temperatures.

The linear relationship of $\Delta T_B$ on $\beta_q - \beta_T$ for all 1600 stretched profiles shows two differences for HIRS and AMSU-B (Figure 5.2c). First, the slope of the relationship is weaker for HIRS. One reason for this is the expected influence of the reduced pressure broadening. Another reason is the lower sensitivity of $\Delta T_B$ to changes in $\beta_T$ for HIRS (Figure 5.2a). Second, the mean value of $\Delta T_B$ is higher for HIRS. The reason is the additional positive bias in $\Delta T_B$ for $\beta_q > 1$. Stretching the profiles equally, this positive bias leads to a stronger increase of $\Delta T_B$ for HIRS.

The differences between HIRS and AMSU-B in the dependence of $\Delta T_B$ that are pointed out in Figure 5.2a and b are also visible in the contour plot in Figure 5.3. For increasing $\beta_q$, the decreasing pressure broadening effect weakens the decrease of $\Delta T_B$ for HIRS. Furthermore, $\Delta T_B$ measured by HIRS is less sensitive to an increase in $\beta_T$ because the shape of the emission layer for HIRS differs from AMSU-B. Both effects, combined with possible additional effects, cause the lines of constant $\Delta T_B$ to be further apart from each other for HIRS. Lines of constant $\Delta T_B$ have a steeper slope for HIRS and diverge slightly for increasing stretching parameters, similar to AMSU-B (Chapter 3). Therefore, a decreasing slope of the linear relationship with increasing stretching parameters as a possible result of the change in the lapse rate is also found for HIRS.

The differences between HIRS and AMSU-B found for the idealized atmospheres (Figure 5.2) agree well with the results using data from the MPI-ESM-LR (Figure 5.4). For the last warm period the correlation between $\Delta T_B$ and $\beta_q - \beta_T$ is similar for HIRS and AMSU-B with high values of -0.93 and -0.94, respectively. As expected from the idealized experiment above, the slope of the linear fit is weaker for HIRS than for AMSU-B and weakens for increasing stretching parameters (Figure A.3), similar to AMSU-B. Furthermore, the mean value of $\Delta T_B$ for the last warm period is less negative for HIRS which might be caused by the reduced pressure broadening.

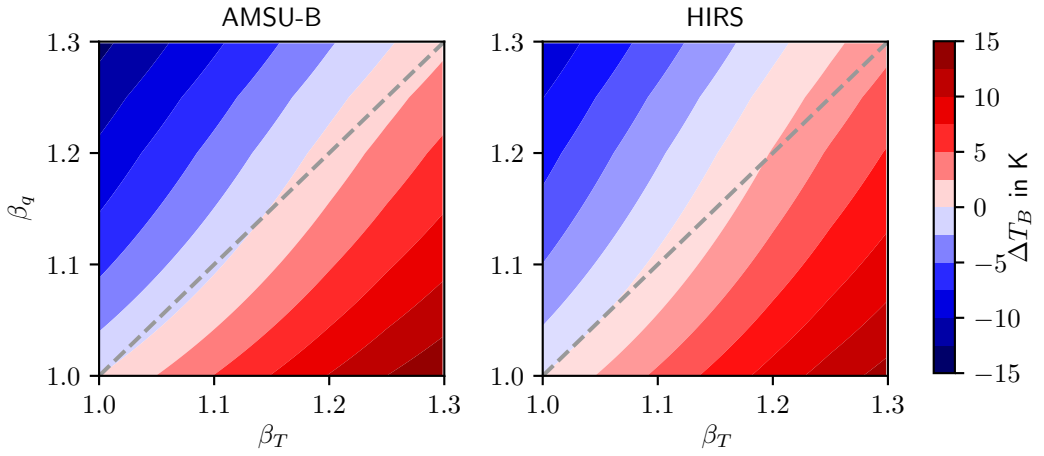


FIGURE 5.3: Dependence of the change in brightness temperature ($\Delta T_B$) on the individual stretching parameters $\beta_T$ for temperature and $\beta_q$ for humidity, simulated for AMSU-B (left panel) and HIRS (right panel). The gray dotted line indicates the one-to-one line.

In conclusion, the new perspective is robust for HIRS and AMSU-B, although the relationship between $\Delta T_B$ and $\beta_q - \beta_T$ differs for both measurement instruments. The negative relationship between $\Delta T_B$ and $\beta_q - \beta_T$ is weaker for HIRS than for AMSU-B. One reason for this is the difference in the weighting functions within the emission layer, which leads to a lower sensitivity of $\Delta T_B$ on a vertical stretching for HIRS. Additionally, it seems plausible that the reduction of pressure broadening for an upward shift of the emission layer mainly affects HIRS and further reduces the sensitivity. However, these factors might not be the only reasons for the difference in sensitivity for HIRS. In any case, it should be kept in mind that $T_B$ changes differently for both instruments when applying the new perspective to satellite measurements.

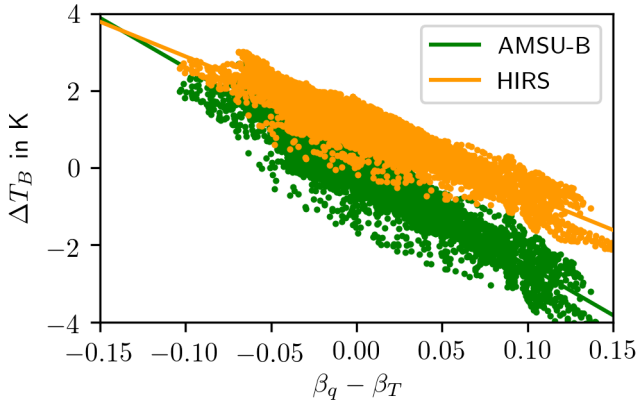


FIGURE 5.4: Dependence of the change in brightness temperature ($\Delta T_B$) on the difference of the optimized stretching parameters ($\beta_q - \beta_T$) for all tropical grid cells for the last warm period (years 110–140) in the MPI-ESM-LR for AMSU-B (green) and HIRS (orange).

# Chapter 6

# Conclusions

The brightness temperature ($T_B$) of the upper troposphere is measured for water vapor channels in the infrared and microwave region. The traditional view is that $T_B$ corresponds to the relative humidity in the upper troposphere. I developed a new perspective on the change of the brightness temperature $\Delta T_B$ in a warming climate. The new perspective connects $\Delta T_B$ with a vertical stretching of the specific humidity ($q$) and ($T$) profiles. Vertical stretching is a process which is able to describe a major part of the atmospheric profiles changes in a warming climate. The new perspective allows to interpret $\Delta T_B$ not only as a function of a change in the relative humidity, but also as a consequence of a different evolution of the $T$ and $q$ profiles.

First, I investigated the dependence of $\Delta T_B$ in an idealized experiment by stretching one $T$ and $q$ profile individually and calculating the corresponding $\Delta T_B$. There is a strong linear dependence of $\Delta T_B$ on the difference of the respective stretching parameters for $T$ and $q$. When $q$ is stretched stronger than $T$, $\Delta T_B$ is negative. A stronger stretching of $T$ causes a positive $\Delta T_B$. The values of $\Delta T_B$ for a similar stretching of $T$ and $q$ are small even though they increasingly deviate from zero with increasing stretching parameters. Furthermore, the sensitivity of $\Delta T_B$ to a vertical stretching decreases with increasing stretching parameters. This is likely caused by a decrease in the temperature lapse rate due to vertical stretching.

Second, I showed that stretching is a good approximation of the $T$ and $q$ profiles actual evolution in the CMIP5 model MPI-ESM-LR. Within a layer between 400 and 200 hPa the error of the stretched profiles compared to the actual profile normalized with $\Delta T$ is below 7% for most $T$ profiles and below 18% for $q$. The corresponding optimal stretching parameters for $q$ are variable in their spatial distribution and temporal evolution. In contrast, the stretching parameters for $T$ are distributed very homogeneous and evolve uniformly. However, the tropical means of both stretching parameters evolves similarly.

Third, I investigated if the new perspective is applicable for the MPI-ESM-LR. To do so, I calculated the optimal stretching parameter for every $T$ and $q$ profile in the tropics. I showed that the new perspective is applicable for the MPI-ESM-LR. The correlation of $\Delta T_B$ and the difference of the stretching parameters is strong with values even below -0.9 towards the end of the time series. The dependence of $\Delta T_B$ on the difference of the stretching parameters in the model is similar to the idealized experiment, even though a bit weaker. As in the idealized experiment the dependence of $\Delta T_B$ on a vertical stretching weakens with increasing stretching parameters.

Fourth, I tested the robustness of the results across 20 models of the CMIP5 ensemble. The new perspective is applicable for all used models with high correlation values for the last warm period below -0.8 for almost all models. This is an encouraging result, having

in mind that the spatial distribution and temporal evolution of the stretching parameters and $\Delta T_B$ have a wide spread across the models. The slope of the linear connection between $\Delta T_B$ and the stretching parameters is depending on the models climate sensitivity.

Additionally, I tested the robustness of the new perspective for two different measurement instruments AMSU-B and HIRS. The applicability of the new perspective is independent of the measurement instrument that is used for the simulations of $T_B$. However, the sensitivity of $\Delta T_B$ on the difference of the stretching parameters is weaker for HIRS. A possible reason for that is the reduced pressure broadening caused by an upward shift of the emission layer which influences HIRS stronger than AMSU-B. This should be kept in mind when it comes to comparing satellites measurements of $\Delta T_B$ to model data.

The aim of this thesis was to introduce a new perspective on $\Delta T_B$ by connecting it to a vertical stretching of the $T$ and $q$ profiles. The new aspect of this perspective is that it does not rely on interpreting the absolute values of $T_B$ in order to interpret its change $\Delta T_B$. Instead, it focuses on directly interpreting $\Delta T_B$ by connecting it to a process of vertical stretching which is able to describe a major part of the evolution of the $T$ and $q$ profiles in a warming climate in all models used in this thesis. I showed that the new perspective is robust and applicable across 20 CMIP5 climate models. The new perspective offers an alternative view which can be used to interpret $\Delta T_B$ in a warming climate and it opens up new possibilities to evaluate climate model predictions.

# Appendix A

# Appendix

## A.1 Availability of the script code

All scripts used in this thesis, are written in python and are available on request. This includes a python wrapper for the radiative transfer model RTTOV. For access to the scripts, please contact me at `lau_die@gmx.de`.

## A.2 Supplementary Figures

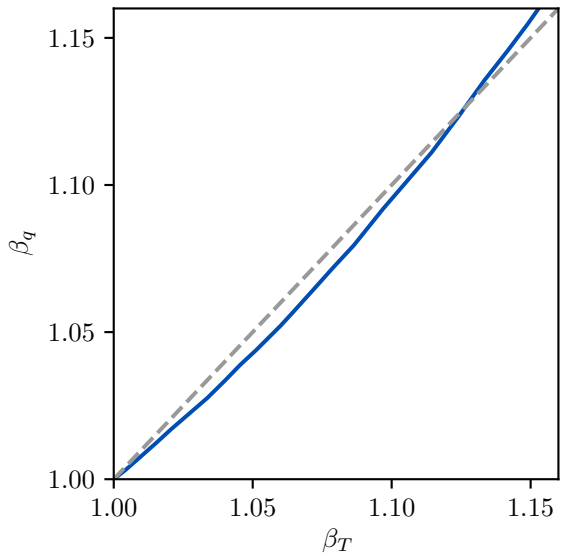


FIGURE A.1: Evolution over all 17 warm periods of the tropical mean of the optimal stretching parameters for temperature ($\beta_T$) and for specific humidity ($\beta_q$) in the MPI-ESM-LR. The gray dotted line indicates the one-to-one line.

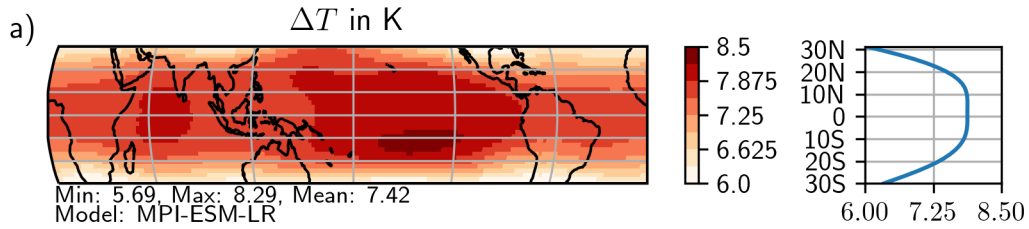


FIGURE A.2: Change in temperature $\Delta T$ averaged over the optimization layer (400–200 hPa) from the control period (0–30) to the last warm period (110–140) in the MPI-ESM-LR.

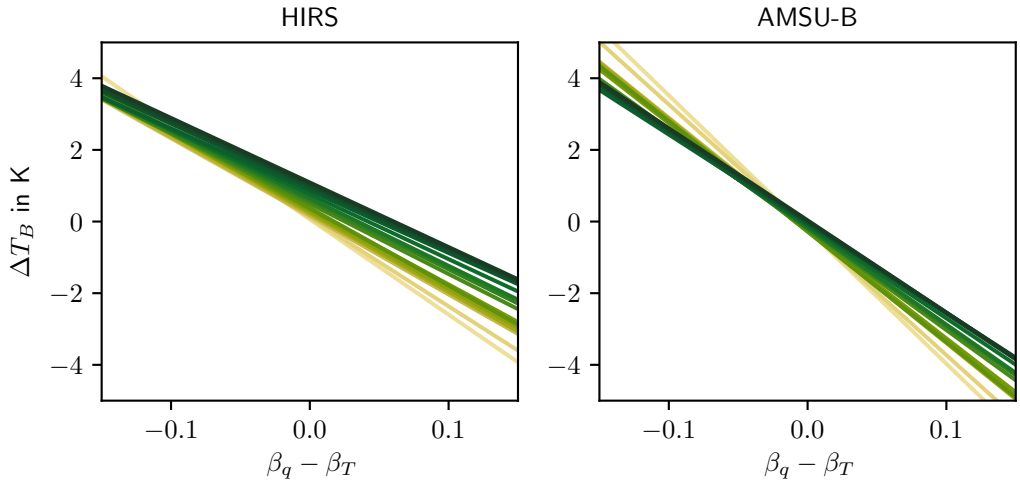


FIGURE A.3: Linear fit of the change in brightness temperature ($\Delta T_B$) with respect to the difference of the optimal stretching parameters for the specific humidity and temperature $\beta_q - \beta_T$ for all 17 warm periods between the years 30–60 (beige line) and the years 100–140 (dark green line) in the MPI-ESM-LR for HIRS (left panel) and AMSU-B (right panel).

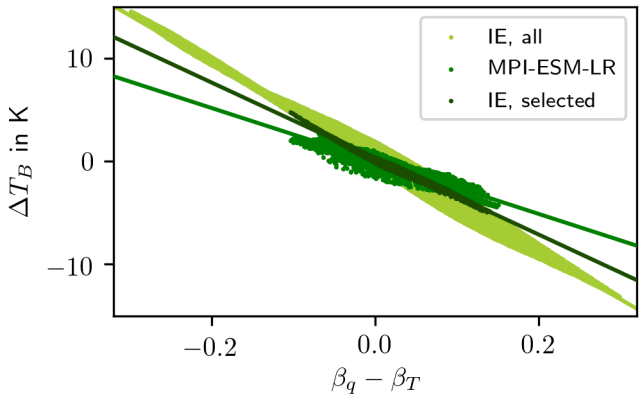


FIGURE A.4: Change in brightness temperature ($\Delta T_B$) as a function of the difference of the optimal stretching parameters for the specific humidity and temperature $\beta_q - \beta_T$ and the corresponding linear fits for all profiles in the idealized experiment (bright green, Chapter 3), the MPI-ESM-LR model data for th last warm period (years 110–140) (green) and for profiles in the idealized experiment which correspond to a similar stretching as in the last warm period in the MPI-ESM-LR (dark green).

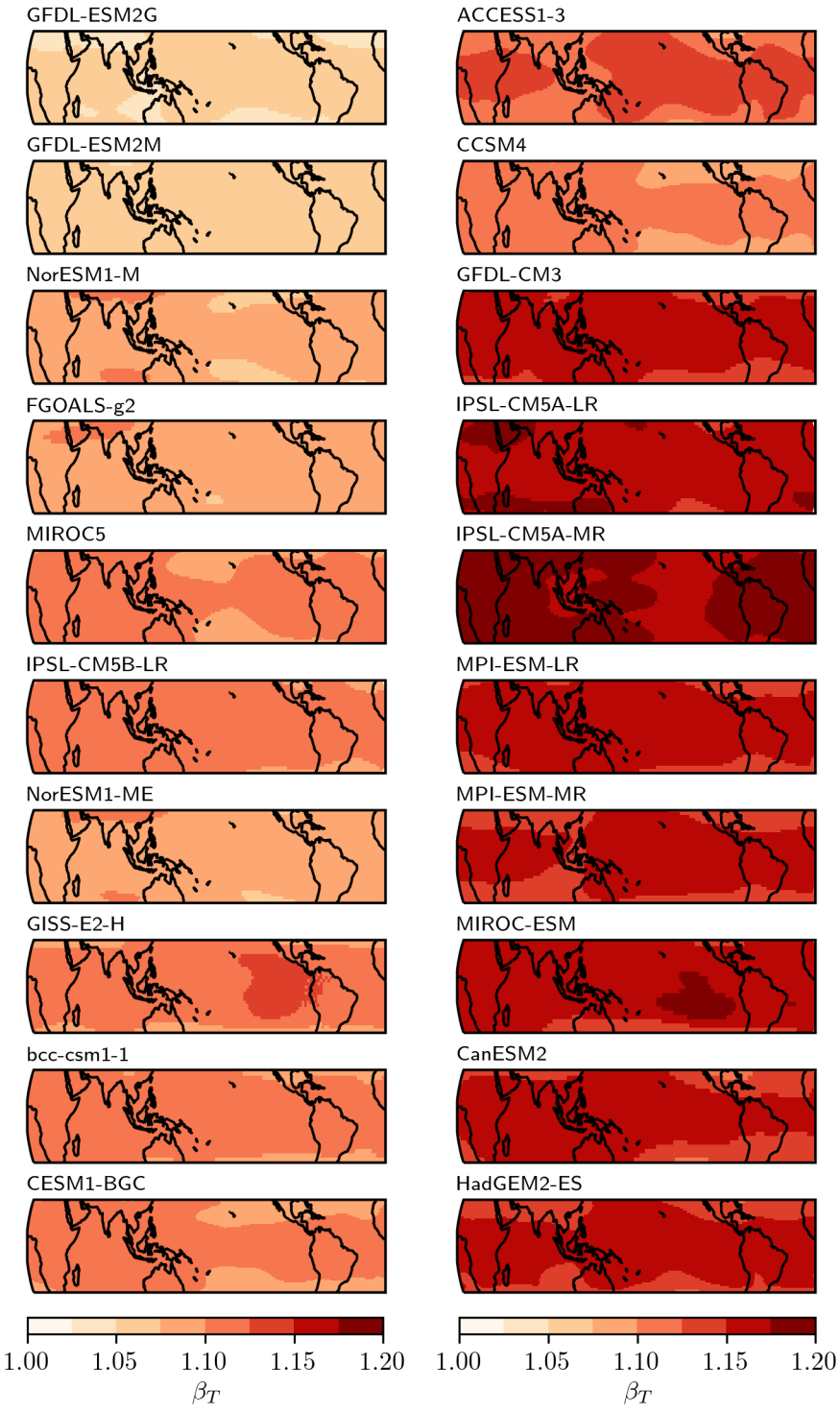


FIGURE A.5: Optimal stretching parameters ($\beta_T$) for temperature profiles for 20 different CMIP5 models. The models are sorted by their transient climate response (TCR) from low to high TCR values.

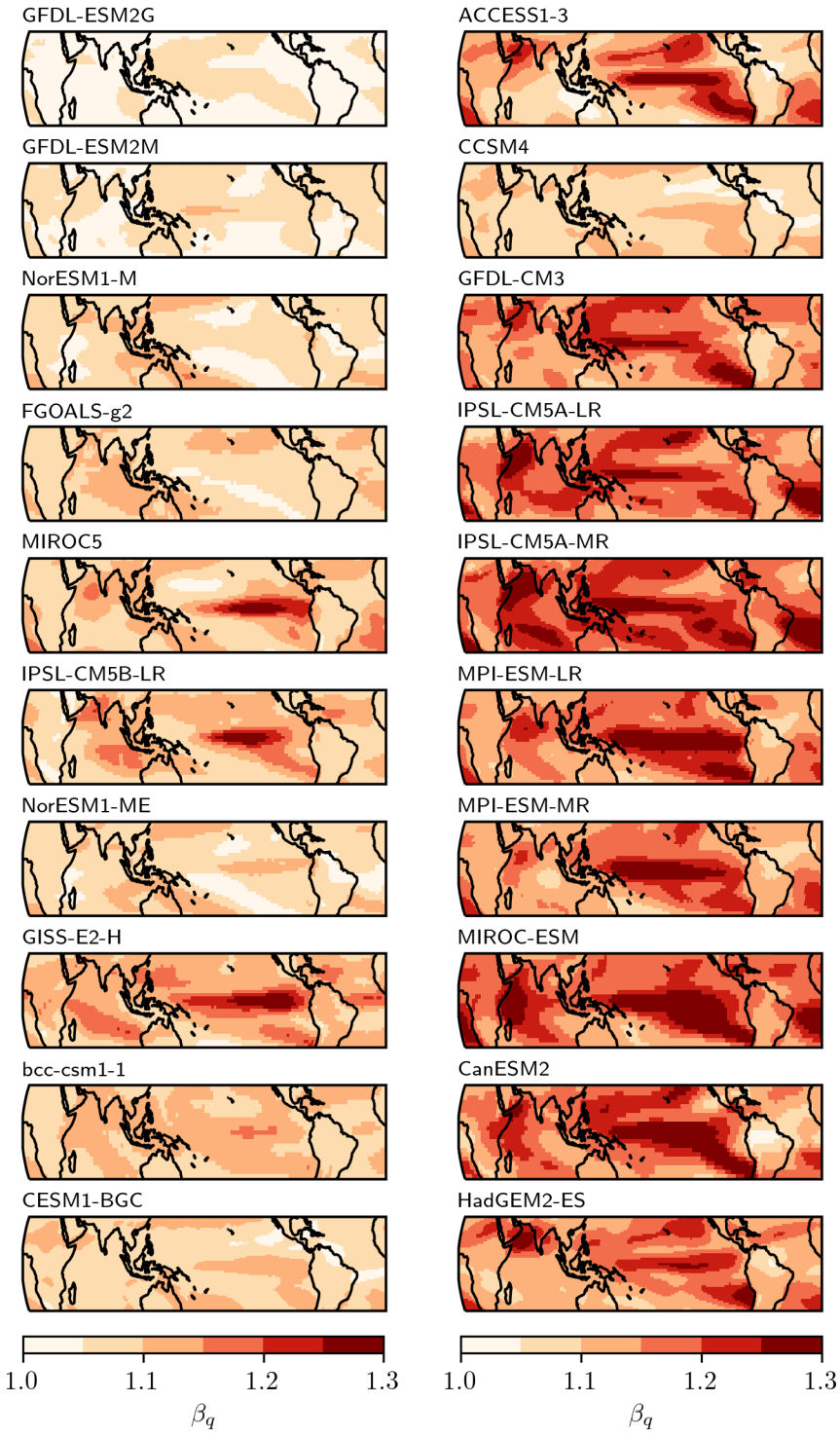


FIGURE A.6: Optimal stretching parameters ($\beta_q$) for specific humidity profiles for 20 different CMIP5 models. The models are sorted by their transient climate response (TCR) from low to high TCR values.

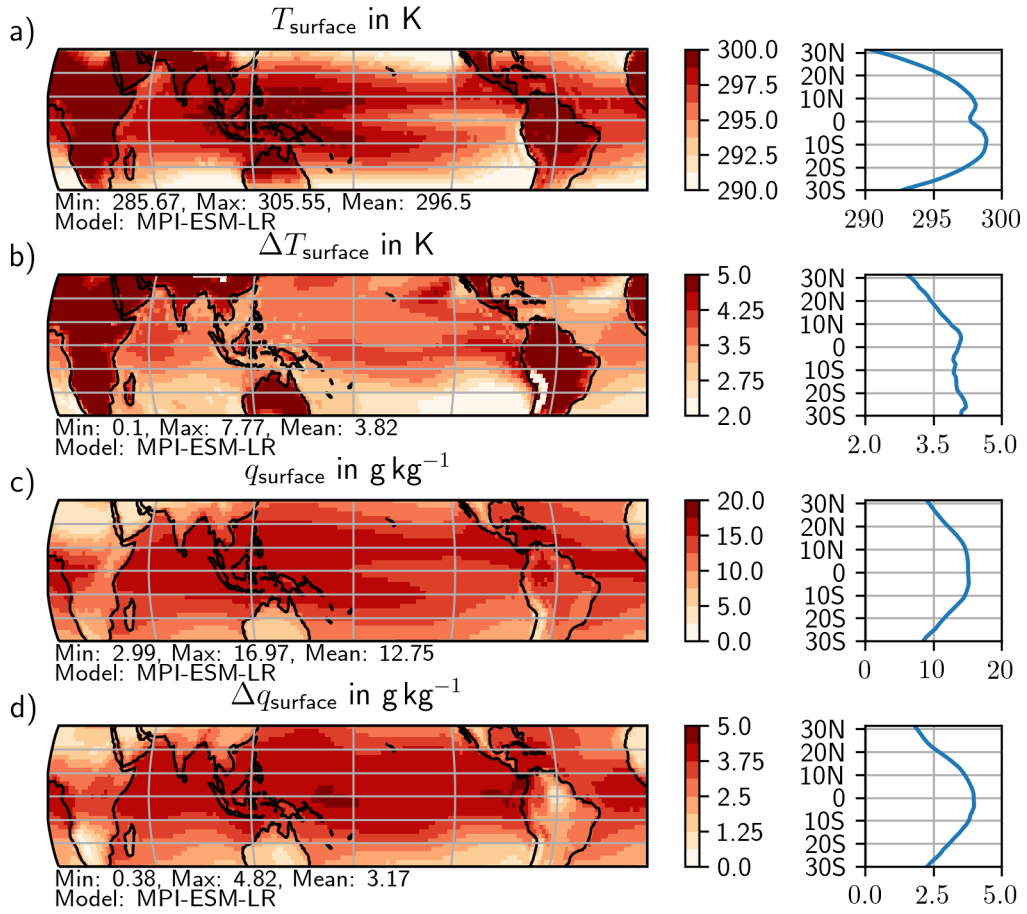


FIGURE A.7: Surface temperature ($T_{\text{surface}}$, a) and its change ($\Delta T_{\text{surface}}$, b) between the last warm period (years 110–140) and the control period (years 0–30) in the MPI-ESM-LR. Same for the surface specific humidity ($q_{\text{surface}}$, c) and its change ($\Delta q_{\text{surface}}$, d).

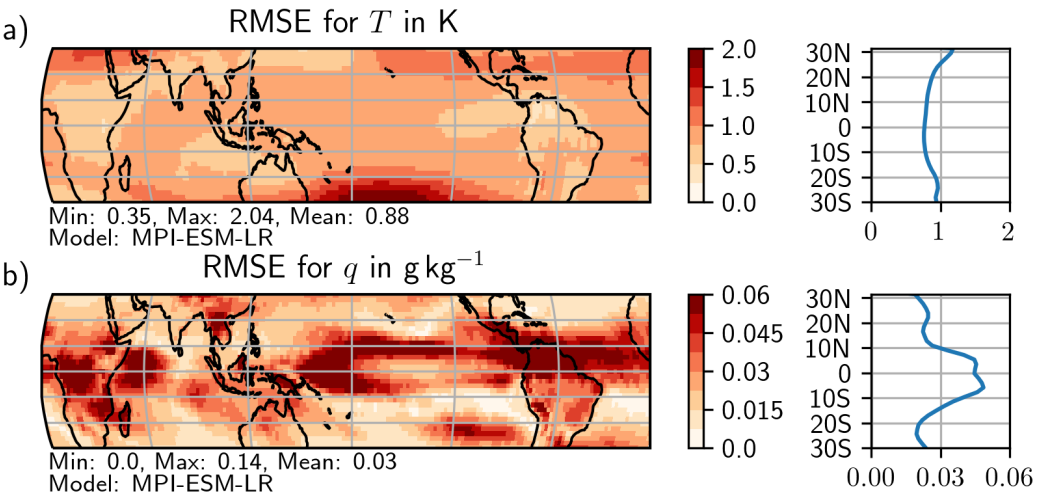


FIGURE A.8: Root-Mean-Square Error (RMSE) averaged over the optimization layer (400–200 hPa) between the stretched and the warm profiles for temperature ($T$, a) and specific humidity ($q$, b) in the MPI-ESM-LR

# Bibliography

Baranger, M. (1958). "General Impact Theory of Pressure Broadening". In: *Physical Review* 112.3, pp. 855–865.

Bretherton, A. H. Sobeland C. S. (2000). "Modeling Tropical Precipitation in a Single Column". In: *Journal of Climate* 13.24, pp. 4378–4392. DOI: 10.1175/1520-0442(2000)013<4378:MTPIAS>2.0.CO;2.

Buehler, S. A. and V. O. John (2005). "A Simple Method to Relate Microwave Radiances to Upper Tropospheric Humidity". In: *Journal of Geophysical Research* 110, D02110. DOI: 10.1029/2004JD005111.

Buehler, S. A., P. Eriksson, T. Kuhn, A. von Engeln, and C. Verdes (2005). "ARTS, the atmospheric radiative transfer simulator". In: *Journal of Quantitative Spectroscopy and Radiative Transfer* 91.1, pp. 65–93. DOI: 10.1016/j.jqsrt.2004.05.051.

Buehler, S. A., J. Mendrok, P. Eriksson, A. Perrin, R. Larsson, and O. Lemke (2018). "ARTS, the atmospheric radiative transfer simulator — version 2.2, the planetary toolbox edition". In: *Geoscientific Model Development* 11.4, pp. 1537–1556. DOI: 10.5194/gmd-11-1537-2018.

Byrne, M. P. and T. Schneider (2016). "Narrowing of the ITCZ in a warming climate: Physical mechanisms". In: *Geophysical Research Letters* 43.21, pp. 11350–11357. DOI: 10.1002/2016GL070396.

Byrne, Michael P and Paul A O'Gorman (2013). "Link between land-ocean warming contrast and surface relative humidities in simulations with coupled climate models". In: *Geophysical Research Letters* 40.19, pp. 5223–5227.

Byrne, Michael P, Angeline G Pendergrass, Anita D Rapp, and Kyle R Wodzicki (2018). "Response of the intertropical convergence zone to climate change: Location, width, and strength". In: *Current climate change reports* 4.4, pp. 355–370.

Cai, W., S. Borlace, M. Lengaigne, P. van Rensch, M. Collins, G. Vecchi, A. Timmermann, A. Santoso, M. J. McPhaden, L. Wu, M. H. England, G. Wang, E. Guilyardi, and F.-F. Jin (2014). "Increasing frequency of extreme El Niño events due to greenhouse warming". In: *Nature climate change* 4, pp. 111–116. DOI: 10.1038/NCLIMATE2100.

Dalu, Gianni (1986). "Satellite remote sensing of atmospheric water vapour". In: *International Journal of Remote Sensing* 7.9, pp. 1089–1097.

Dessler, A. E., Z. Zhang, and P. Yang (2008). "Water-vapor climate feedback inferred from climate fluctuations, 2003-2008". In: *Geophysical Research Letters* 35, L20704. DOI: 10.1029/2008GL035333.

Eriksson, P., S. A. Buehler, C. P. Davis, C. Emde, and O. Lemke (2011). "ARTS, the atmospheric radiative transfer simulator, Version 2". In: *Journal of Quantitative Spectroscopy and Radiative Transfer* 112.10, pp. 1551–1558. DOI: 10.1016/j.jqsrt.2011.03.001.

Flato, Gregory, Jochem Marotzke, Babatunde Abiodun, Pascale Braconnot, S Chan Chou, William Collins, Peter Cox, Fatima Driouech, Seita Emori, Chris Eyring Veronika Forest, Peter Gleckler, Eric Guilyardi, Christian Jakob, Vladimir Kattsov, Chris Reason, Markku Rummukainen, et al. (2014). "Evaluation of Climate Models". In: *Climate Change 2013: The Physical Science Basis. Contribution of Working Group I to the Fifth Assessment*

*Report of the Intergovernmental Panel on Climate Change*. Cambridge University Press, pp. 741–866.

Fu, Qiang, Syukuro Manabe, and Celeste M Johanson (2011). "On the warming in the tropical upper troposphere: Models versus observations". In: *Geophysical Research Letters* 38.15.

Giorgetta, Marco A, Johann Jungclaus, Christian H Reick, Stephanie Legutke, Jürgen Bader, Michael Böttinger, Victor Brovkin, Traute Crueger, Monika Esch, Kerstin Fieg, et al. (2013). "Climate and carbon cycle changes from 1850 to 2100 in MPI-ESM simulations for the Coupled Model Intercomparison Project phase 5". In: *Journal of Advances in Modeling Earth Systems* 5.3, pp. 572–597.

Held, I. M. and B. J. Soden (2000). "Water Vapor Feedback and Global Warming". In: *Annual review of energy and the environment* 25, pp. 441–475.

Hsu, Pang-chi, Tim Li, Jing-Jia Luo, Hiroyuki Murakami, Akio Kitoh, and Ming Zhao (2012). "Increase of global monsoon area and precipitation under global warming: A robust signal?" In: *Geophysical Research Letters* 39.6.

Huang, Y., V. Ramaswamy, and B. Soden (2007). "An investigation of the sensitivity of the clear-sky outgoing longwave radiation to atmospheric temperature and water vapor". In: *Journal of Geophysical Research: Atmospheres* 112.D5.

Jiang, J. H., H. Su, C. Zhai, V. S. Perun, A. Del Genio, L. S. Nazarenko, L. J. Donner, L. Horowitz, C. Seman, J. Cole, A. Gettelman, M. A. Ringer, L. Rotstayn, S. Jeffrey, T. Wu, F. Brient, J.-L. Dufresne, H. Kawai, T. Koshiro, M. Watanabe, T. S. L'Ecuyer, E. M. Volodin, T. Iversen, H. Drange, M. D. S. Mesquita, W. G. Read, J. W. Waters, B. Tian, J. Teixeira, and G. L. Stephens (2012). "Evaluation of cloud and water vapor simulations in CMIP5 climate models using NASA "A-Train" satellite observations". In: *Journal of Geophysical Research* 117, D14105. DOI: 10.1029/2011JD017237.

John, V. O. and B. J. Soden (2007). "Temperature and humidity biases in global climate models and their impact on climate feedbacks". In: *Geophysical Research Letters* 34, L18704. DOI: 10.1029/2007GL030429.

John, V. O., G. Holl, R. P. Allan, S. A. Buehler, D. E. Parker, and B. J. Soden (2011). "Clear-sky biases in satellite infra-red estimates of upper tropospheric humidity and its trends". In: *Journal of Geophysical Research* 116, D14108. DOI: 10.1029/2010JD015355.

Kim, Seon Tae and Jin-Yi Yu (2012). "The two types of ENSO in CMIP5 models". In: *Geophysical Research Letters* 39.11.

Kushner, Paul J, Isaac M Held, and Thomas L Delworth (2001). "Southern Hemisphere atmospheric circulation response to global warming". In: *Journal of Climate* 14.10, pp. 2238–2249.

Lang, T. (2019). "A new Climate Data Record of Upper Tropospheric Humidity". MA thesis. Universität Hamburg, Fachbereich Geowissenschaften, Meteorologisches Institut.

Lau, William KM and Kyu-Myong Kim (2015). "Robust Hadley circulation changes and increasing global dryness due to CO2 warming from CMIP5 model projections". In: *Proceedings of the National Academy of Sciences* 112.12, pp. 3630–3635.

Manabe, S. and R. J. Stouffer (1980). "Sensitivity of a Global Climate Model to an Increase of CO2 Concentration in the Atmosphere". In: *Journal of Geophysical Research: Oceans* 85.C10, pp. 55290–5554. DOI: 10.1029/JC085iC10p05529.

Manabe, S. and R. T. Wetherald (1967). "Thermal equilibrium of the atmosphere with a given distribution of relative humidity". In: *Journal of the Atmospheric Sciences* 24.3, pp. 241–259. DOI: 10.1175/1520-0469(1967)024<0241:TEOTAW>2.0.CO;2.

Mokhov, II and MG Akperov (2006). "Tropospheric lapse rate and its relation to surface temperature from reanalysis data". In: *Izvestiya, Atmospheric and Oceanic Physics* 42.4, pp. 430–438.

O'Gorman, Paul A and Martin S Singh (2013). "Vertical structure of warming consistent with an upward shift in the middle and upper troposphere". In: *Geophysical Research Letters* 40.9, pp. 1838–1842.

Plesca, E., V. Grützun, and S. A. Buehler (2018). "How robust is the weakening of the Pacific Walker circulation in CMIP5 idealized transient climate simulations?" In: *Journal of Climate* 31.1, pp. 81–97. DOI: 10.1175/JCLI-D-17-0151.1.

Randall, D. A., R. A. Wood, S. Bony, R. Colman, T. Fichefet, J. Fyfe, V. Kattsov, A. Pitman, J. Shukla, J. Srinivasan, R. J. Stouffer, A. Sumi, and K. E. Taylor (2007). "Climate models and their evaluation". In: *Climate Change 2007: The Physical Science Basis. Contribution of Working Group I to the Fourth Assessment Report of the Intergovernmental Panel on Climate Change*. Ed. by S. Solomon, D. Qin, M. Manning, Z. Chen, M. Marquis, K. B. Averyt, M. Tignor, and H. L. Biller. Cambridge, United Kingdom and New York, NY, USA: Cambridge University Press.

Raval, A. and V. Ramanathan (1989). "Observational determination of the greenhouse effect". In: *Nature* 342, pp. 758–761.

Robel, J. et al. (2009). *NOAA KLM User's Guide with NOAA-N, -N' Supplement*. Tech. rep. National Oceanic et al.

Saunders, R. W., T. J. Hewison, S. J. Stringer, and N. C. Atkinson (1995). "The Radiometric Characterization of AMSU-B". In: *IEEE Transactions on microwave theory and techniques* 43.4, pp. 760–771.

Saunders, Roger, James Hocking, Emma Turner, Peter Rayer, David Rundle, Pascal Brunel, Jerome Vidot, Pascale Roquet, Marco Matricardi, Alan Geer, et al. (2018). "An update on the RTTOV fast radiative transfer model (currently at version 12)". In: *Geoscientific Model Development* 11.7, pp. 2717–2737.

Shi, L. and J. J. Bates (2011). "Three decades of intersatellite-calibrated High-Resolution Infrared Radiation Sounder upper tropospheric water vapor". In: *Journal of Geophysical Research* 116, D04108. DOI: 10.1029/2010JD014847.

Singh, M. S. and P. A. O'Gorman (2012). "Upward Shift of the Atmospheric General Circulation under Global Warming: Theory and Simulations". In: *Journal of Climate* 25, pp. 8259–8276. DOI: 10.1175/JCLI-D-11-00699.1.

Soden, B. J. and F. P. Bretherton (1993). "Upper Tropospheric Relative Humidity From the GOES 6.7 $\mu$m Channel: Method and Climatology for July 1987". In: *Journal of Geophysical Research* 98.D9, pp. 16,669–16,688.

Soden, B. J. and I. M. Held (2006). "An assessment of climate feedbacks in coupled ocean-atmosphere models". In: *Journal of Climate* 19.14, pp. 3354–3360. DOI: 10.1175/JCLI3799.1.

Soden, B. J., D. J. Jackson, V. Ramaswamy, M. D. Schwarzkopf, and X. Huang (2005). "The Radiative Signature of Upper Tropospheric Moistening". In: *Science* 310.5749, pp. 841–844. DOI: 10.1126/science.1115602.

Sohn, Byung-Ju, Sang-Wook Yeh, Ahreum Lee, and William KM Lau (2019). "Regulation of atmospheric circulation controlling the tropical Pacific precipitation change in response to CO 2 increases". In: *Nature communications* 10.1, p. 1108.

Spencer, R. W. and W. D. Braswell (1997). "How Dry is the Tropical Free Troposphere? Implications for Global Warming Theory". In: *Bulletin of the American Meteorological Society* 78.6, pp. 1097–1106.

Stevenson, SL (2012). "Significant changes to ENSO strength and impacts in the twenty-first century: Results from CMIP5". In: *Geophysical Research Letters* 39.17.

Taylor, K. E., R. J. Stouffer, and G. A. Meehl (2012). "An Overview of CMIP5 and the Experiment Design". In: *Bulletin of the American Meteorological Society* 93.4, pp. 485–498. DOI: 10.1175/BAMS-D-11-00094.1.

Thomas, Gary E and Knut Stamnes (2002). *Radiative transfer in the atmosphere and ocean*. Cambridge University Press.

Trenberth, K. E., J. Fasullo, and L. Smith (2005). "Trends and variability in column-integrated atmospheric water vapor". In: *Climate dynamics* 24, pp. 741–758.

Wang, Bin, So-Young Yim, June-Yi Lee, Jian Liu, and Kyung-Ja Ha (2014). "Future change of Asian-Australian monsoon under RCP 4.5 anthropogenic warming scenario". In: *Climate dynamics* 42.1-2, pp. 83–100.

Zelinka, M. D. and D. L. Hartmann (2010). "Why is longwave cloud feedback positive?" In: *Journal of Geophysical Research: Atmospheres* 115.D16, p. D16117. DOI: 10.1029/2010JD013817,.

# Acknowledgements

I would like to thank a number of people for their support and the contribution to the completion of my Master's thesis.

My special thanks goes to Prof. Dr. Stefan Bühler for introducing me to the topic of my Master's thesis and for all the time he devote to discuss my results and create next steps. I've learned a lot about scientific work and research, as well as writing scientific writing from him.

I also want to give special thanks to Lukas Kluft who highly supported me, particularly in the last challenging months of my Master's thesis. He taught me the subtleties of scientific writing and how to present my results the clearest. I further would like to thank him for carefully reading and checking my thesis.

Moreover, I want to thank Dr. Verena Grützun for introducing me in the radiative transfer model RTTOV and for having her door always open, supporting me, especially in all the small issues I had in the begin of my work.

I want to thank all members of the "Radiation and Remote Sensing" working group for providing me with new ideas, especially Theresa Lang for helping and advising me intensively. I always enjoyed it to be part of the group and would like to thank for the pleasant working atmosphere.

Furthermore, I would like to thank my fellow students Theresa Lang, Jakob Dörr, Marc Prange, Simon Michel, Joscha Fregin and Daniel Sorg for the inspiring discussions, the enjoyable lunch times and for checking my final thesis.

For having made it possible for me to study meteorology, for all constructive words and for all relaxing days at home I would like to thank my family.

Last but not least, I want to thank my boyfriend Jakob for the great support, all suggestions, helping me to keep motivated and reading carefully through my Master's thesis. I couldn't have got through without him.

# Versicherung an Eides statt

Hiermit versichere ich an Eides statt, dass ich die vorliegende Arbeit im Studiengang M.Sc. Meteorologie selbstständig verfasst und keine anderen als die angegebenen Hilfsmittel – insbesondere keine im Quellenverzeichnis nicht benannten Internet-Quellen – benutzt habe. Alle Stellen, die wörtlich oder sinngemäß aus Veröffentlichungen entnommen wurden, sind als solche kenntlich gemacht. Ich versichere weiterhin, dass ich die Arbeit vorher nicht in einem anderen Prüfungsverfahren eingereicht habe und die eingereichte schriftliche Fassung der auf dem elektronischen Speichermedium entspricht.

Mit einer Ausstellung der Arbeit in der Fachbibliothek bin ich einverstanden.

| | |
|---|---|
| Ort, Datum | Laura Dietrich |